Modeling spatiotemporal dynamics of global wetlands: Comprehensive evaluation of a new sub-grid TOPMODEL parameterization and uncertainties

Zhen Zhang[1,2,3], Niklaus E. Zimmermann[1,4] , Jed O. Kaplan[5], Benjamin Poulter[2]
[1]Dynamic Macroecology, Swiss Federal Research Institute WSL, Zürcherstrasse 111, 8903 Birmensdorf, Switzerland
[2]Institute on Ecosystems and Department of Ecology, Montana State University, Bozeman, MT 59717, United States of America
[3] Cold and Arid Regions Environmental and Engineering Research Institute, Chinese Academy of Sciences, Lanzhou, 730000, Gansu, China
[4] Department of Environmental Systems Science, Swiss Federal Institute of Technology ETH, 8092 Zürich, Switzerland
[5] Institute of Earth Surface Dynamics, University of Lausanne, 1015 Lausanne, Switzerland

Abstract: Simulations of the spatiotemporal dynamics of wetlands are key to understanding the role of wetland biogeochemistry under past and future climate. Hydrologic inundation models, such as TOPography-based hydrological model (TOPMODEL), are based on a fundamental parameter known as the *compound topographic index (CTI)* and offer a computationally cost-efficient approach to simulate wetland dynamics at global scales. However, there remains large discrepancy in the implementations of TOPMODEL in land-surface models (LSMs) and thus their performance against observations. This study describes new improvements to TOPMODEL implementation and estimates of global wetland dynamics using the LPJ-wsl ("Lund-Potsdam-Jena WSL version") Dynamic Global Vegetation Model (DGVM), and quantifies uncertainties by comparing three digital elevation model (DEM) products (HYDRO1k, GMTED, and HydroSHEDS) at different spatial resolution and accuracy on simulated inundation dynamics. In addition, we found that calibrating TOPMODEL with a benchmark wetland dataset can help to successfully delineate the seasonal and interannual variation of wetlands, as well as improve the spatial distribution of wetlands to be consistent with inventories. The HydroSHEDS DEM, using a river-basin scheme for aggregating the CTI, shows best accuracy for capturing the spatiotemporal dynamics of wetlands among the three DEM products. The estimate of global wetland potential/maximum is ~ 10.3 Mkm^2 (10^6 km^2), with a mean annual maximum of ~ 5.17 Mkm^2 for 1980-2010. When integrated with wetland methane emission submodule, the uncertainty of global annual CH_4 emissions from topography inputs is estimated to be 29.0 Tg yr^{-1}. This study

demonstrates the feasibility of TOPMODEL to capture spatial heterogeneity of inundation at large scale and highlights the significance of correcting maximum wetland extent to improve modeling of interannual variations in wetland area. It additionally highlights the importance of an adequate investigation of topographic indices for simulating global wetlands and shows the opportunity to converge wetland estimates across LSMs by identifying the uncertainty associated with existing wetland products.

Keywords: Seasonal wetland dynamics, DGVM, LPJ, methane emission, Topographic index, Compound topography index (CTI)

Introduction

For their ability to emit the greenhouse gas methane (CH_4), wetland ecosystems play a disproportionately important role in affecting the global climate system through biogeochemical feedbacks (Fisher et al., 2011; Seneviratne et al., 2010). Wetlands are thought to be the largest natural source of CH_4 emission by contributing 20-40% of the total annual emissions to atmosphere, which adds a strong radiative forcing from CH_4 (Bousquet et al., 2006; IPCC, 2013). The seasonal and interannual distribution of wetland area remains one of the largest uncertainties in the global CH_4 budget (Kirschke et al., 2013), in particular for the roughly 60% of wetlands that are not inundated permanently (Petrescu et al., 2010). Changes in the spatial extent of seasonally inundated wetlands was most likely a major driver for CH_4 variations during last glacial period (Kaplan, 2002) and are considered as an important driver of the strong atmospheric CH_4 growth rate resumed in 2007 (Nisbet et al., 2014) and in future climate change scenarios (Stocker et al., 2013).

Improving our understanding of the role of wetlands in global greenhouse-gas (GHG) budgets requires a representation of wetlands and their biogeochemical processes in land surface models (LSM) to both hindcast observed past variations (Singarayer et al., 2011) and to predict future trajectories in atmospheric CH_4 and terrestrial C balance (Ito and Inatomi, 2012; Meng et al., 2012; Spahni et al., 2011; Stocker et al., 2014; Zürcher et al., 2013). Dynamic wetland schemes in LSMs were based on conceptual theories and physical processes describing surface water processes (e.g., infiltration and evapotranspiration) and water movement in the soil column using probability distributions derived from subgrid topographic information (Beven and Kirkby, 1979), or using analytical functional parametric forms with fixed parameters (Liang et al., 1994). Currently, the most common approach for global wetland modelling is to use a runoff simulation scheme such as TOPMODEL (TOPography-based hydrological MODEL) (Beven and Kirkby, 1979; Kleinen et al., 2012; Ringeval et al., 2012; Zhu et al., 2014), which includes the assumption that lateral soil water transport driven by topography follows the same

exponential decline as the vertical decrease in hydraulic conductivity within soil profiles in a basin (Sivapalan et al., 1987).

TOPMODEL-based implementations have proven successful at capturing the broad geographic distribution of wetlands and their seasonal variability (Gedney and Cox, 2003; Ringeval et al., 2012; Stocker et al., 2014; Zhu et al., 2014), but have consistently overestimated both the extent of wetlands and duration of inundation at global and regional scale when compared with existing current surveys (Junk et al., 2011; Prigent et al., 2007; Quiquet et al., 2015). For instance, simulations using the Earth system model HadGEM2 predict much larger persistent Amazonian wetlands than an inventory (Collins et al., 2011). In general, independently determined wetland area using hydrologic modules of LSMs in The Wetland and Wetland CH_4 Inter-comparison of Models Projects (WETCHIMP) experiment simulated larger global wetland extent than those informed by remotely sensed product and inventories (Melton et al., 2013). This large disagreement also exists across specific regions (Ringeval et al., 2014). For example, Bohn et al. (2015) carried out a model inter-comparison of wetland extent on the West Siberian Lowland, one of the major wetland regions in high latitudes, and highlighted similar uncertainties of wetland extent simulation in the LSMs participating in the WETCHIMP experiment and using TOPMODEL.

Meanwhile, uncertainties in wetland area estimation partly come from a paucity of observational datasets and different definitions of wetland (Matthews and Fung, 1987). Remotely sensed datasets have difficulties in capturing small or isolated water in saturated soils that are not flooded on the surface (Prigent et al., 2007), as well capturing the forested wetlands that obscure detection of inundation because of dense forest canopies (Bohn et al., 2015). In addition, ground-based survey or inventories that determine wetlands usually limited as static distribution that cannot provide temporal patterns for inundated area, making it hard to evaluate with simulated results. On the other hand, the definition of wetland for regional- or global-scale modelling assumes the land surface has both inundated and saturated conditions, which is not necessarily the same as inundated area measured by satellite observations (Melton et al., 2013).

While prognostic wetland dynamics schemes are promising to resolve these observational issues, the configuration parameters for TOPMODEL are a potential source of uncertainty in estimating wetland dynamics (Marthews et al., 2015). Among all parameters in TOPMODEL, the Compound Topographic Index (CTI) is of critical importance for determining inundated areas in terrain-related hydrological applications (Ward and Robinson, 2000; Wilson and Gallant, 2000). It measures the tendency of soils to become saturated (Beven and Cloke, 2012) and consequently it drives the accuracy of wetland area scaled to the larger grid

cell (Ducharne, 2009; Mulligan and Wainwright, 2013). Although the importance of CTI has been highlighted, only few studies have so far evaluated the effect of CTI on modelling the spatial and temporal patterns of global wetland dynamics. This is due to a limited availability of global CTI products. During the last decade, the first CTI product at 1km resolution from HYDRO1k global dataset released by U.S. Geological Survey (USGS) in 2000 has become the most commonly applied global dataset for large-scale applications (Kleinen et al., 2012; Lei et al., 2014; Ringeval et al., 2012; Wania et al., 2013). However, HYDRO1k has been proven to potentially overestimate inundation extent due to a lack in quality of the underlying digital elevation model (DEM) (Grabs et al., 2009; Lin et al., 2010; Lin et al., 2013; Sørensen and Seibert, 2007;). With recent advances in the development of DEMs (Danielson and Gesch, 2011; Lehner et al., 2008), there is a both a requirement and an opportunity to investigate uncertainties caused by CTI parameter.

The primary goal of our study is to improve the modeling of dynamically varying wetland extents with i) a parameter constraint to match integrated satellite and inventory observations, and with ii) a better parameterizations of CTI values for determining wetland seasonal cycles using new topographic data and aggregation schemes (i.e., grid versus catchment). To this end, we develop a new version of Dynamic Global Vegetation Model (DGVM) LPJ-wsl ("Lund-Potsdam-Jena WSL version") that includes the TOPMODEL approach for wetland extent modelling by also accounting for soil thermal dynamics and high-latitude soil-water freeze and thaw cycles, and by incorporating the necessary physical processes (e.g. snow aging) that constrain global wetland dynamics. We utilize three commonly used global DEM products to evaluate the effects of sub-grid parameterizations on simulated global wetland extent uncertainties. We perform six global simulations resulting from the combination of three DEM products and two aggregation schemes under the same common experimental protocol. The specific aims are: (1) to improve the performance of estimated wetland extent based on TOPMODEL for the purpose of large-scale modelling, (2) to develop a new parameterization scheme using inventory in combination with satellite-based retrievals, and (3) to evaluate the uncertainties and the spatial and temporal differences of CTI from three major DEM products in model behavior.

2 Model Descriptions and Experimental Design

The model LPJ-wsl is a process-based dynamic global vegetation model developed for carbon cycle applications based on development of the LPJ-DGVM (Sitch et al., 2003). LPJ-wsl includes land surface processes, such as water, carbon fluxes, and vegetation dynamics that are intimately represented by plant functional types (PFTs) (Poulter et al., 2011). The distribution of PFTs is simulated based on a set of bioclimatic limits and by plant-specific parameters that govern the competition for resources. The soil hydrology is modeled using

semi-empirical approach, with the soil treated as bucket consisting of two layers each with fixed thickness (Gerten et al., 2004). The LPJ-wsl CH_4 model used in this study is the same as presented in Hodson et al., (2011) and is a function of two scaling factors ($r_{CH4:C}$ and f_{ecosys}), soil temperature, soil-moisture-dependent fraction of heterotrophic respiration, and wetland extent according to the following equation:

$$E(x,t) = r_{CH4:C} \cdot f_{ecosys}(x) \cdot A(x,t) \cdot R_h(x,t) \quad (1)$$

where $E(x,t)$ is wetland CH_4 flux, $A(x,t)$ is wetland extent, $R_h(x,t)$ is heterotrophic respiration, f_{ecosys} is a scaling factor representing different wetland ecosystems, $r_{CH4:C}$ is the ratio C to CH_4 fluxes.

LPJ-wsl has been evaluated in previous studies using global inventory datasets and satellite observations and has been one of the participating models in the WETCHIMP study (Melton et al., 2013). Modifications made here to the original LPJ-wsl model and a detailed description of changes are summarized below:

- A permafrost module that simulate soil freeze and thaw processes, is implemented and modified following the Wania et al. (2009) study (see description in Sect. 2.1).
- The snow module from Wania et al. (2009) was included and modified to include some of the effects of snow ageing on snow thermal properties. We use an updated parameterization of soil thermal properties both for the permafrost and the snow module, which is calibrated by satellite observations specifically for global application.
- A new parameterization of soil texture was formulated based on the Harmonized World Soil Database (HWSD), which combines the recently collected extensive volumes of regional and national updates of soil parameter information (Nachtergaele et al., 2008). The new soil texture in LPJ-wsl follows the U.S. Department of Agriculture soil classification with 14 soil types grouped according to a particular range of particle-size fractions (e.g. sand, clay, loam, etc.), instead of using the original Food and Agriculture Organization of the U.N. classification with 9 soil types (Sitch et al., 2003). Thus, the volumetric water holding capacity, also defined as potential maximum soil water content (SWC), is assumed to vary spatially, calculated as a function of the surface soil texture using pedotransfer functions from Cosby et al., 1984. Wilting point, porosity, mineral soil content and organic soil content for each soil type are derived from a look-up table available from the Air Force Weather Agency (2002) as listed in Table 1.

The modified LPJ-wsl version is thus the starting point upon which the TOPMODEL-based wetland and permafrost modules are included (Sect. 2.2).

2.1 Permafrost Model

In order to consider the functional wetland area extension during the spring thaw and their shrinking or disappearances during autumn freeze, we added to

LPJ-wsl a soil temperature scheme and freeze-thaw processes, as in Wania et al. (2009). The modified version considers the soil heat capacity and its thermal conductivity, which are both affected by the volumetric fractions of the soil physical components, such as water-ice fraction, mineral soil, or peat. The thermal scheme of LPJ-wsl is discretized vertically using 8-layers of variable thickness, while the water-balance scheme is kept the same as the original LPJ-DGVM, which means the daily changes in water content are allocated to the "old" upper and lower layer of LPJ while considering percolation between these two layers and baseflow from the lower layer. Fractional water and ice content in each of the 8-layers is calculated on a daily time step. Soil temperature is updated in the thermal routine and then passed to the hydrological routine to determine the water-ice phase change in permafrost routine.

2.2 Dynamic Wetland Model

To represent the grid cell fraction covered by wetlands, we have implemented an approach based on the TOPMODEL hydrological framework (Beven and Kirkby, 1979). TOPMODEL was initially developed to operate at the scale of large watersheds using the channel network topography and dynamics contributing areas for runoff generation, and was later extended to perform over areas that are much larger than a typical river catchment (Gedney and Cox, 2003). The fundamental information to determine the area fraction with soil water saturation is derived from knowledge of the mean watershed water table depth and a probability density function (PDF) of combined topographic and soil properties (Sivapalan et al., 1987). The CTI, which provides the sub-grid scale topographic information in TOPMODEL, determines the likelihood of a grid box to be inundated. It is defined as:

$$\lambda_l = \ln\left(\frac{\alpha_l}{tan\beta_l}\right) \quad (2)$$

where λ_l represents local CTI value, α_l represent the contributing area per unit contour, $\tan\beta_l$, the local topographic slope, approximates the local hydraulic gradient where β is the local surface slope. The CTI distribution can be generated from digital elevation models and near global datasets are readily available, e.g. HYDRO1k dataset from USGS.

Following the central equations of TOPMODEL, the relationship between local water table depth z_l and the grid mean water table depth z_m can be given as:

$$\lambda_l - \lambda_m = f\{z_l - z_m\} \quad (3)$$

where λ_m is the mean CTI averaged over the grid box, f is the saturated hydraulic conductivity decay factor with depth for each soil type. This equation is valuable in that it relates the local moisture status to the grid box mean moisture status based on the subgrid-scale variations in topography. Higher CTI values than average are indicative of areas with higher water table depth than average water table, and vice versa. We therefore calculate the inundated areas

(F_{wet}) of all the sub-grid points within a grid cell that have a local water table depth z_l >= 0:

$$F_{wet} = \int_{z_l}^{z_{max}} pdf(\lambda) d_\lambda \quad (4)$$

where instead of using the CTI values themselves, we followed a common up-scaling approach to approximate the distribution of CTI values within a grid cell in order to reduce computation costs. Here, the discrete distribution of the CTI for lowland pixels (i.e. $\lambda_l \geq \lambda_m$) has been represented as an exponential function, not as a three-parameter gamma distribution as applied in recent applications for modeling wetland extent (Kleinen et al., 2012; Ringeval et al., 2012). As shown in Figure 1, the new exponential function agrees well with the three-parameter gamma distribution function when the CTI is larger than the mean CTI λ_m. This change allows linking the inundated fraction directly to water table depth, thus improving the parameterization by providing physical meaning and fewer calibration parameters. This change also improves the parameterization of fractional saturated area, especially in mountainous regions (Niu et al., 2005).

Finally, the wetland area fraction (F_{wet}) is represented as:

$$F_{wet} = F_{max} e^{-C_s f(\lambda_l - \lambda_m)} \quad (5)$$

Where C_s is a coefficient representing the topographic information generated by fitting the exponential function to the discrete cumulative distribution function (CDF) of the CTI. F_{max} is the maximum wetland fraction of a grid cell. Because of the uncertainties involved in determining the water table depth, the hydraulic factor f, and the coarse resolution DEMs, the maximum soil saturated fraction calculated from discrete CDF are prone to large uncertainties and thus complicate the comparison of the saturated fraction with existing observations (Ducharne, 2009; Ringeval et al., 2012). Here, we introduce a calibration of maximum wetland fractions F_{max}. We used the inventory-calibrated satellite observations (see description in 3.3) combining with inventory dataset to calculate representative long-term maximum wetland extents within each grid box (0.5°), i.e. the parameter F_{max} for each grid cell i:

$$F_{max_i} = \max(\mathrm{A_{GLWD_i}}, \max(\mathrm{A_{SWAMP-GLWD_i}})) \quad (6)$$

$\mathrm{A_{GLWD}}$ represents wetland estimate from GLWD, and $\mathrm{A_{SWAMP\text{-}GLWD}}$ represents long-term wetland estimate from SWAMPS-GLWD. The reason for combining these two datasets is to take the advantage of satellite-based observations at capturing temporal wetlands and inventory-based datasets at estimating forested wetlands and small wetlands ignored by remote sensing. This calibration is also based on the assumption that water is stagnant within local grids at large scale, in particular for model using simple 'bucket' concept to calculate grid-mean water table depth.

In addition, we used nonlinear least squares (nls) estimates to fit the discrete CDF curve of CTI for lowlands ($\lambda_l < \lambda_m$) to calculate parameter C_s, the parameter

that determines varying trend of wetland extent. By this, the parameters F_{max}, λ_m and C_s for determining inundated areas are derived (Figure 2).

To account for the permafrost effects on soil infiltration properties, we followed Fan and Miguez-Macho (2011) and Kleinen et al. (2012) who modified f by a function k depending on January temperature T_{jan}. Since LPJ-wsl uses two soil layers from the HWSD soil texture database (Nachtergaele et al., 2008) to represent the different texture characteristics, the modification depends on the combination of a look-up table (Table 1) from soil types and water table depth:

$$k = \begin{cases} 1 & \forall T_{jan} > -5℃ \\ 1.075 + 0.015T_{jan} & -25℃ < \forall T_{jan} < -5℃ \\ 0.75 & \forall T_{jan} < -5℃ \end{cases} \quad (7)$$

Since the observed CH_4 emission during winter are mainly attributed to physical processes during soil freezing effects (Whalen and Reeburgh, 1992), for the partially frozen wetland in high latitudes, we introduced an effective fraction of wetland area (F_{wet}^{eff}) defined by:

$$F_{wet}^{eff} = \left(\frac{\omega_{liq}}{\omega_{liq}+\omega_{froz}}\right)_{50\ cm} \cdot F_{wet} \quad (8)$$

where ω_{liq} and ω_{froz} are the fraction of liquid and frozen soil water content in the upper soil (0-0.5 m) respectively. Since the liquid water content in the lower soil layer gets trapped and cannot contribute to CH_4 emission when upper soil is frozen, we didn't consider the lower layer for surface wetland calculations.

3 Experimental set-up and datasets

3.1 Topographic information

In this study we used three DEMs of varying spatial resolution, HYDRO1k at 30 arc-second (USGS, 2000; http://lat.cr.usgs.gov/HYDRO1K), Global Multi-resolution Terrain Elevation Data 2010 (GMTED) at 15 arc-second (Danielson and Gesch, 2011), and HydroSHEDS at 15 arc-second (Lehner et al., 2008) to compare the effect of sub-grid topographic attributes on simulated seasonal and interannual variability of wetlands. HYDRO1k, developed from the USGS released 30 arc-second digital elevation model of the world (GTOPO30), is the first product that allowed spatially explicit hydrological routines applied in large-scale applications (USGS, 2000). HydroSHEDS, developed from satellite-based global mapping by the Shuttle Radar Topography Mission (SRTM), is a significant improvement in the availability of high- resolution DEMs covering all land areas south of 60°N (the limit of SRTM). For the areas at higher latitudes we used HYDRO1k by aggregating the GTOPO30 DEM to provide global grids. GMTED was produced using seven data sources including SRTM, global Digital Terrain Elevation Data (DTED), Canadian elevation data, Spot 5 Reference3D data, and data from the Ice, Cloud, and land Elevation Satellite (ICESat), covering nearly all global terrain.

To avoid mismatch of CTI value inherent in computing CTI with different CTI algorithms, we generated three global CTI maps based on the three DEM products, instead of relying on existing CTI products (e.g. HYDRO1k CTI, HydroSHEDS CTI product from Centre for Ecology and Hydrology) (Marthews et al., 2015). Since studies show that multiple flow direction algorithms for calculating CTI give better accuracy compared with single-flow algorithms in flat areas (Kopecký and Čížková, 2010; Pan et al., 2004), thus we selected an algorithm from R library 'topmodel' (Buytaert, 2011), which applies the multiple flow routing algorithm of Quinn et al. (1995) to calculate the global CTI maps. The DEMs from HYDRO1k and HydroSHEDS had been previously processed for hydrological-correction, meaning that the DEMs were processed to remove elevation depressions that would cause local hydrologic 'sinks'. To include a comparison of (hydrologically) corrected and uncorrected DEMs in our analyses as some studies have been done previously (Stocker et al., 2014), the GMTED DEM was applied without hydrological correction.

3.2 Description of the simulation

For running LPJ-wsl with permafrost and TOPMODEL, we used global meteorological forcing (temperature, cloud cover, precipitation and wet days) as provided by the Climatic Research Unit (CRU TS 3.22) at 0.5° resolution (Harris et al., 2014). To spin up the LPJ-wsl model using the CRU climatology, climate data for 12-months were randomly selected from 1901-1930 and repeated for 1000 years with a fixed pre-industrial atmospheric CO_2 concentration. The first spinup simulation started from initial soil temperature derived from LPJ-wsl simulated results on January 1901 and continued with a land use spin-up simulation. These procedures ensure that carbon stocks and permafrost are in equilibrium before performing transient simulations. The transient simulations, with observed climate and CO_2 were performed with monthly climate disaggregated to daily time steps over the 1901-2013 period. The 1993-2013 years were used for evaluation against satellite data and inventories.

One of key assumptions in TOPMODEL is that the water table is recharged at a spatially uniform and steady rate with respect to the flow response timescale of the catchment (Stieglitz et al., 1997). Given the fact that we consider the water to be stagnant within each grid, the mean CTI parameter was estimated with two alternative schemes: (1) a regular 'grid-based' or gridded approach, i.e., the subgrid CTI values were averaged per 0.5° grids, and (2) an irregular 'basin-based' approach, where mean CTI were calculated over the entire catchment area in which the respective pixel is located. For generating a global catchment map at 0.5° resolution, we applied a majority algorithm in the case of multi-catchments in a grid with consideration of avoiding isolated pixels for specific river basin. There are two catchment area products applied in this study, HYDRO1k (2013) and HydroSHEDS. Similarly, the parameter C_s was generated

using nonlinear least squares estimates from both of these two different CTI calculation strategies. Two sets of model experiments were carried out to compare the wetland dynamics under basin and grid-based TOPMODEL parameterizations respectively (Table 2).

3.3 Evaluation and benchmarking data

Since the soil freeze-thaw cycles are a key component for determining seasonal cycles of wetlands in cold regions, in this study we benchmarked the general pattern of permafrost locations by comparing the model output against satellite observations of freeze and thaw status and inventories of permafrost extent. Since soil depth in LPJ-wsl is held at 2.0 m for the permafrost module, the permafrost extent in this study is defined as the lower soil (0.5-2 m) that is always at or below the freezing point of water 0°C for multiple years. The permafrost extent map at 0.5-degree resolution from National Snow and Ice Data Center (NSIDC) is adopted for benchmarking (Brown et al., 2001). The global dataset of Freeze/Thaw (FT) status is derived from satellite microwave remote sensing provided by the Numerical Terradynamic Simulation Group (NTSG) at University of Montana and is based on daily maps over a 34-year record (1979-2012). It represents the FT status of the composite landscape vegetation-snow-soil medium to constrain surface water mobility and land-atmosphere carbon fluxes (Kim et al., 2012).

Two global inundation products derived from satellite observations were additionally used for evaluation purposes: the Global Inundation Extent from Multi-Satellites (GIEMS), derived from visible (AVHRR) and active (SSM/I) and passive (ERS) microwave sensors over the period 1993-2007; the Surface Water Microwave Product Series (SWAMPS), derived from active (SeaWinds-on-QuikSCAT, ERS, and ASCAT) and passive (SSM/I, SSMI/S, AMSR-E) microwave sensors over the period 1992-2013. This new SWAMPS global dataset, hereby denoted as SWAMPS-GLWD, was first developed at NASA JPL (Schroeder et al., In preparation). We re-scaled this dataset with the Global Lake and Wetland Database (GLWD) (Lehner and Döll, 2004), a well-established global inventory of water bodies at high resolution to match SWAMPS-GLWD with the inventory estimates. This post-processed SWAMPS product covers the required regions for forested wetlands, which are not readily observable by passive or active microwave measurements (Poulter, et al., in preparation). For evaluating regional wetland patterns, we selected two study areas (the largest peatland West Siberian Lowland (WSL); the largest floodplain, Amazon River Basin). Three wetland map products over the WSL from (Sheng et al., 2004), (Peregon et al., 2008) and (Tarnocai et al., 2009) (denoted by “Sheng2004”, “Peregon2008”, Tarnocai2009 respectively) and one up-date high resolution dual-season inundated area inventory for lowland Amazon basin from Japanese Earth Resources Satellite (JERS-1) were applied (Hess et al., 2015) (denoted by

"Hess2015"). We aggregated all above-mentioned datasets from the native 25 km to a 0.5-degree spatial resolution and from daily to monthly temporal resolution for comparison with model outputs (Table A1).

4 Results

4.1 Evaluation against observations

We first evaluated the permafrost module that constrains the seasonal cycles of wetland area in cold regions with respect to inventory and remote sensing observations. Figure 3a compares the spatial distribution of permafrost extent from inventory and the modeled permafrost extent over the period 1980-2000. Figure 3b gives the spatial distribution of spearman rank correlation between the simulated and observed number of monthly frozen-days. The modeled permafrost extent shows high agreement with benchmarking dataset, with a slightly higher coverage of permafrost regions in North-Western Eurasia. The model successfully captures the seasonally frozen soil, which is closely linked to surface wetland formation and seasonal variation of wetland in cold regions. Most of the regions reveal a temporal correlation > 0.9, while Eastern Siberia and the Southern permafrost distribution edge is generally around 0.5. The lower correlation in East Siberia probably originates from two issues: high snow depth in LPJ-wsl that insulates soil temperature and consequent delay of soil temperature to reach complete freezing; and the relatively large uncertainty of FT-ESDR derived soil frozen status in those regions (Kim et al., 2012). This difference can be partly explained by the different representation of frozen status between simulated results and satellite retrievals. Remotely sensed maps reflect the mixed condition of the upper vegetation canopy, snow layer and surface soil, while the simulated frozen days only represent the frozen state of topsoil.

Figure 4 illustrates the model evaluation at the regional scale over the West Siberian Lowland (Figure 4). The model generally captures the spatial extent of the seasonal maximum wetland area fraction across the whole WSL for the JJA season successfully. However, the TOPMODEL approach without calibration (denoted as 'Original') shows large areas with relatively low wetland proportion and cannot capture high values. This suggests poor model performance in simulating wetland areas without F_{max} calibration. The calibrated model generally exhibits good agreement with inventories and satellite retrievals. It is especially successful at capturing the spatial heterogeneity of wetland areal extent over the whole WSL regions. LPJ-wsl simulated results reveal additional wetland area in the northeast, where wetlands entirely lacked in the GLWD map, although captured in other datasets. Meanwhile, LPJ-wsl captured the higher wetland area in region between 61 and 66°N and 70 and 80°E regions compared with GLWD, where mire/bog/fen was dominated across that region. LPJ-wsl also maintained well the spatial pattern of wetlands in forested region south of 60°N,

which was captured by inventories (Sheng2004, Peregon2008, and GLWD), but was missed by two satellite products (SWAMPS-GLWD, GIEMS) due to the limitation of remotely sensed datasets in detecting water under vegetative canopy and/or due to reduced sensitivity.

As illustrated in Figure 5, LPJ-wsl captured the spatial pattern of simulated wetlands well with lower estimates of the total wetland area in low-water season compared to the JERS-1 observed maps. Differences between Hess2015 and LPJ-wsl maps were primarily in two regions, Maranon-Ucayali region of Peru (MUP, 3-7°S, 73-77°W) and Llanos de Moxos in Bolivia (LMB, 11-17°S, 60-68°W). LPJ-wsl shows higher wetland coverage in MUP while Hess2015 indicates high wetland fraction in LMB in high-water season. Global satellite products largely ignore the LMB region that was partly captured in LPJ-wsl, indicating that LPJ-wsl using hybrid TOPMODEL approach can yield estimates closer to those of fine-resolution mapping, while large-scale satellite products are likely to underestimate Amazon wetland extent because of their coarse spatial resolution that limit the ability to detect inundation outside of large wetlands and river floodplains (Hess et al., 2015).

To evaluate the effect of F_{max} calibration on CH_4 emission estimates, two estimates of CH_4 (with and w/o calibration) over the WSL regions were compared with observation-based estimate from Glagolev et al. (2011) (Figure 6). The 3-year mean annual total emission from original version is 6.29±0.51 Tg CH_4 yr^{-1}, falling into the upper part of range from land surface models and inversions (Bohn et al., 2015), whereas the calibrated version is close to the estimate of Glagolev et al. (2011) (3.91±1.29 Tg CH_4 yr^{-1}) with 4.6±0.45 Tg CH_4 yr^{-1},. In addition, the spatial pattern of CH_4 emission with F_{max} calibration shows better agreement with observation than non-calibration one with relatively larger emissions in Taiga forests and central region (55-65°N, 65-85°E). We also compared our estimates with recent airborne campaign observations for Alaska during 2012 growing season. Estimates with F_{max} calibration also falls well into the range of recent estimate (2.1±0.5 Tg CH_4 yr^{-1}) for Alaska based on airborne observations (Chang et al., 2014) with a total of 1.7 Tg CH_4 yr^{-1} during 2012 growing season (3.1 Tg CH_4 yr^{-1} from non-calibrated estimate), indicating the necessity to calibrate F_{max} to accurately capture annual CH_4 emission and spatial variability for boreal wetlands.

4.2 Spatial distribution

Several observations applicable to evaluate the difference among sub-grid parameterizations of TOPMODEL are available for the WSL region. Figure 7 lists the spatial patterns of simulated JJA (June-July-August) wetland area over WSL regions to illustrate differences among wetland maps. The general patterns of wetland extent are substantially similar, because they both used the same calibrated F_{max} map. Both of these datasets show wetlands distributed across most of the WSL, with extensive wetlands in the central region (55-65°N, 60-90°E). However, the detailed pattern is differing between the approaches and

DEMs used, which indicate the uncertainty of parameterizations on wetland distribution. The basin-based parameterization can capture the higher wetland areas in regions with bog, mire, or fen vegetation in the central east (63-67°N, 85-90°E) as was found in the GLWD benchmark map. The grid-based parameterizations fail to reproduce this pattern. It seems that the grid-based parameterizations are less sensible in capturing the spatial heterogeneity throughout most of the WSL. The difference in parameterization derived from DEM datasets also affects the simulated regional pattern. Both of HydroSHEDS-based results successfully reproduce the high wetland fractions in the southern-forested regions (55-60°N, 65-80°E), while HYDRO1k and GMTED both cannot capture this feature. Note that GMTED is derived from the same DEM product SRTM as HydroSHEDS but without hydro-correction, indicating the importance of hydro-correction in simulating spatial patterns of wetlands.

The comparison of simulated mean annual minimum, maximum, and amplitude of wetland extent with observational datasets (Table 3) reveals that the simulated wetland area for 1980-2010 falls within the range of 4.37±0.99 Mkm^2 ($Mkm^2=10^6$ km^2). This number is close to GIEMS (5.66 Mkm^2) (Prigent et al., 2012) and inventory-based estimates (6.2 Mkm^2) (Bergamaschi et al., 2007) after exclusion of other water bodies like lakes, rivers, and rice paddies (Leff et al., 2004). Considering potential underestimation of satellite-based observation in forested regions, the realistic estimate could possibly be in the upper part of our range. Note that one must be careful when directly comparing model results with the observational datasets based on inventories or digitized maps, because these datasets might represent the long-term maximal area as wetland potential. The higher seasonal wetland extent in GIEMS compared with LPJ-wsl could be partly due to permanent wetlands that are difficult to detect by GIEMS. Lastly, the definition of wetland is another possible source of discrepancy. Remotely sensed inundation datasets emphasizes on open water while wetland area in our study is specifically defined from inventories following the National Wetlands Working Group (1988) classification that include peatlands, mineral wetlands, and seasonally inundated shallow waters.

4.3 Seasonal cycle

The shapes of the seasonal patterns in wetland area are generally similar in model simulation compared to satellite observations, despite disagreement in the timing of the seasonal cycle of wetland area in some boreal regions (Figure 8). The modeled results show slightly larger wetland areas in the SON (Sept-Nov) months than satellite-based observations. The larger seasonal wetland areas during SON may originate from the longer periods of unfrozen and relatively water saturated soil in the model data. It thus seems realistic that the satellite-based inundation product AMSR-E observed a similar trend of seasonal inundation patterns for North America and Boreal Eurasia (Jennifer et al., 2014).

This is also supported by field studies in boreal regions, indicating that water table depth during the SON months is still in a high level and soil temperature is above freezing status (Rinne et al., 2007; Turetsky et al., 2014). In contrast, the modeled seasonal cycle of wetland in tropical and temperate regions show a good agreement with GIEMS and SWAMPS-GLWD. Given the difficulties of satellite-based observations in detecting wetlands in forested regions and the reduced sensitivity where open water fraction is low (<10%) (Prigent et al., 2007), the inundation numbers by GIEMS might slightly underestimates the area compared with the simulated results.

Figure 8 reveals that the six data sets of monthly wetland extent for 1993-2007 based on different TOPMODEL parameterization show the same general behavior in the different regions. The six data sets are highly correlated, with largest differences at the maximal wetland extents during growing seasons, especially in the boreal regions. In addition, the differences in seasonal cycle among the six model experiments are relatively small, mostly below 5% regardless of the month. This indicates that the averaged total wetland area is not dependent on the introduction of the new sub-grid parameterizations at the global scale. Among the DEM datasets, HYDRO1k shows the largest difference between basin and grid-based estimates with annual mean wetland area of 89,663 km^2 in boreal regions, while HydroSHEDS has a lowest difference of 6550 km^2 between the two versions. Examining the seasonal amplitude for basin-based schemes, HydroSHEDS shows a better agreement with satellite-based observations than the other two datasets.

4.4 Interannual variability

For evaluating the performance of all the sub-grid parameterizations, we calculated the Pearson's correlation coefficient (r) between modeled and satellite-based results (Table 4). Generally, the comparison demonstrates that simulated interannual variability shows a good agreement with GIEMS and SWAMPS-GLWD in most regions as defined in Fig. 2. For boreal and tropical regions, all correlation coefficients are ranging from 0.7-0.8. The comparison of the inter-annual trends (Figure A1) indicates that absolute values of simulated interannual variations are close to satellite-based observation with good agreement in shape and timing in these regions. This demonstrates the ability of TOPMODEL to capture the large-scale variations in wetland/inundation. Highest disagreements are found in temperate regions that are strongly affected by human activities (likely strong global anthropogenic effect on continental surface freshwater), which is indicated by GIEMS (Prigent et al., 2012) but not by modeled results.

The interannual variability originating from six different sub-grid DEM parameterizations is very similar between these schemes with Spearman rank

correlation coefficient r > 90%. Among the six schemes, the parameters calculated from HydroSHEDS using basin-based statistics result in better agreement between simulated and measured wetland area than the other schemes. In most regions, the SWAMPS-GLWD and GIEMS are consistent in their observed wetland area patterns, except for temperate regions (e.g. Temperate South America, Temperate North America, Europe). This confirms that the differences in surface water extent detection between GIEMS and SWAMPS-GLWD, which might be caused by observational behaviors from different satellite instruments and algorithms. In addition, parameters estimation based on river basins are slightly better than grid-based results.

5.Discussion

5.1 Wetland modelling based on TOPMODEL concept

The coupling between LPJ-wsl and TOPMODEL with calibrated parameters as described in this study, improves the dynamic simulation of wetlands, in particular their geographic location and extent. This is based on the recent discussions of the suitability of TOPMODEL applications to simulate wetland variations at large spatial scale (Ringeval et al., 2012), and intercomparisons of the wetland-area-driven model bias in CH_4 emission at regional scale (Bohn et al., 2015). The large discrepancies of wetland area among LSMs so far have shown extensive disagreement with inventories and remotely sensed inundation datasets (Melton et al., 2013), which is partly due to large varieties of schemes used for representing hydrological processes, or due to the inappropriate parameterizations for simulating inundations. Our results suggest that benchmarking F_{max} is necessary for global wetland modelling.

The simulation of hydrological dynamics within LSMs remains relatively simple because the physical processes described in LSMs occur at much finer spatial scales (Ducharne, 2009; Mulligan and Wainwright, 2013). The coupling of TOPMODEL with process-based LSMs allows for retrieving of the maximum saturated fraction (F_{max}), which is defined by the pixels with no water deficit estimated from the partial integration of the spatial distribution of CTI in a catchment. The estimated distribution of F_{max} is much larger than that obtained from the satellite-based observations (Papa et al., 2010). As a key parameter for determining the soil saturated area, the calculation of F_{max} at large scale is prone to large uncertainties, in particular linked to uncertainties in topographic information, as well as the hydrological processes implemented in large-scale LSMs. Ringeval et al. (2012) pointed to the difficulty of two-layer bucket hydrological model in estimating the mean deficit to the saturation over each grid-cell. This can lead to nonrealistic absolute values of the contributing area in a watershed. We constructed several strategies for optimizing F_{max} by correcting topographic information to match the wetland inventories (Gedney and Cox, 2003; Kleinen et al., 2012). This is one possible solution for global wetland

637 modeling as it assumes that wetland area can be considered constant at coarse
638 spatial resolution (e.g. 0.5° or 1°), following the classical approach of Beven and
639 Kirkby (1979). However, due to the uncertainties from topographic information
640 used in global applications and due to limitations in model parameterizations,
641 this approximation cannot capture the fine scale wetland extent, which
642 complicates the comparison with inventories.
643
644 The integration of satellite-based and inventory-based observations to calibrate
645 F_{max} is highlighted in this study. Combining SWAMPS and GLWD led to simulated
646 wetland area consistent with detailed regional distribution (Poulter et al., in
647 preparation). Our estimation of global wetland potential/maximum is ~ 10.3
648 Mkm^2, and in agreement with the deduction (10.4 Mkm^2) from recent estimates
649 at finer resolution for total open water (~17.3 Mkm^2) (Fluet-Chouinard et al.,
650 2015), lakes (~5 Mkm^2) (Verpoorter et al., 2014), and rice paddies (1.9 Mkm^2)
651 (Leff et al., 2004). The calibration of F_{max} allows for simulating the dynamics of
652 wetland on decade-to-century long time scales. As shown in Figure 9, the
653 wetland potential for permafrost and arid/semi-arid regions is high. Even in
654 tropical regions, there is ~ 20-30% of potential for areas to be inundated.
655
656 According to our evaluation using satellite-based observations and inventories,
657 the spatial distribution of the wetland areas and its temporal variability are
658 generally well captured by our model, both at regional and global scales. In
659 addition, the modeled wetland areas and interannual variability compare well
660 with inventories and satellite-based observations respectively. Unfortunately,
661 the wide disagreement in simulated wetland dynamics among estimates from
662 WETCHIMP hampers our ability to assess model performance (Bohn et al.,
663 2015). Narrowing down the uncertainty of wetland areas by existing maps could
664 minimize the controversial use of the definition between wetlands and
665 inundations. Wetlands have considerable variations in hydrologic conditions,
666 size, locations that make difficult to reconcile a single definitions of wetlands. In
667 current parameterizations, the connectivity of wetlands cannot be represented
668 since wetlands are considered invariant within grid cells.
669
670 **5.2 CTI parameterizations**
671 As shown in this study, global wetland simulations can benefit from improved
672 spatial resolution of topographic maps, thus creating a more realistic
673 representation of processes at sub-grid resolution, and correspondingly better
674 inundation simulations. This is supporting the ideas of Wood et al. (2011) who
675 claimed that higher-resolution modeling leads to better spatial representation of
676 saturated and nonsaturated areas, even though limitations in up-scaling
677 parameterizations may potentially outrun this advantage. The comparison
678 between HydroSHEDS and GMTED also indicated that, for capturing inundated
679 areas under the same spatial resolution, the parameter maps derived from DEM

without hydrological corrections have less accuracy compared to corrected ones (Lehner and Grill, 2013). Without hydrological corrections, valleys would appear as closed depressions in the DEM, leading to an underestimation of inundated areas (Marthews et al., 2015). It could be foreseen that if DEMs in process-based models are being applied at higher resolution, this drawback could be amplified. The comparison between basin- and grid-based parameterizations suggests that grid-based calculations are not appropriate and consequently underestimates wetland areas even when assuming invariant inundated areas at large scale.

The algorithm to calculate CTI is another potential source of error for modelling inundations. The method we applied here is based on calculating a CTI distribution map using a simple algorithm in the R package 'topmodel' instead of using an existing CTI product with improved contributing area. The algorithm we applied using the multi-flow direction algorithm that allows for multiple in-flow and out-flow of water among neighboring pixels when generating topographic values. This could potentially overestimate the contributing areas (Pan et al., 2004). As a result, it might underestimate the wetland areas within each grid cell, and slightly underestimate the temporal pattern of saturated areas because of improper estimates of parameter C_s (Güntner et al., 2004). One limitation of HydroSHEDS is that its projection is not equal-area like HYDRO1k (Marthews et al., 2015), and will cause a potential bias in slope calculation along east-west directions at high latitudes. However, since there is no common method to calculate slope or flow direction, we believe that our calculations provide a reasonable approximation for global applications.

In addition, variability in TOPMODEL parameterizations have considerable influence on simulated CH_4 fluxes, so that the uncertainty of mean annual CH_4 emissions from variable topography inputs is estimated to be 29.0 Tg yr^{-1} (Table 5). Nevertheless, all of the model estimates generally fall within the value range of inversion estimates. The differences of CH_4 emissions among the model experiments is related to simulated magnitude of wetland extents because the fraction of CH_4 emissions from the tropics (~63%) and Extratropics (~27%) remain constant due to the same parameters $r_{C:CH4}$ and f_{ecosys}. The importance of hydrological correction is highlighted by results based on GMTED, suggesting that applying DEMs without hydro-correction may potentially underestimate CH_4 fluxes due to lower hydrological connectivity, which dampen the generation of inundation. In addition, fine-scale topography data like HydroSHEDS reveals higher CH_4 fluxes than HYDRO1k, highlighting the importance to capturing small wetlands/inundated areas that may be ignored by coarse-resolution products.

5.3 Future needs for global wetland modelling

Substantial progress has been made in the development of wetland modeling, but the wide disagreement among estimates from LSMs still exists (Bohn et al., 2015; Melton et al., 2013). Considering that spatiotemporal variation of wetland

725 area can largely influence CH_4 emissions, the selection of appropriate maps
726 needs to be done with care. The parameterization and evaluation of multi-
727 resolution topographic products presented in this study would enhance global
728 wetland modeling if progress could be made in four areas particularly:
729 • *Improved parameters of TOPMODEL for large-scale application*. Our results
730 demonstrate that model simulation after calibrating TOPMODEL are
731 comparable in absolute value with inventories and satellite-based
732 observations at coarser resolution. This supports the ideas of (Beven and
733 Cloke, 2012) that an appropriate scale-dependent subgrid
734 parameterization is the main challenge, regardless of whether it is carried
735 out at global modeling scales or landscape scales. The saturated soil water
736 content is the decisive unit that determines wetland distributions and
737 reasonable estimates of global wetland areas. Hydraulic parameters,
738 which describe soil characteristics for water movement, are critical for
739 modelling wetland seasonal cycles (Marthews et al., 2014). Assessing the
740 uncertainties introduced by aggregating sub-pixel to pixel areas also need
741 to be evaluated.
742 • *Implementing human impact within wetland modeling*. There are
743 evidences from long-term satellite-based observations detecting a
744 significant effect of human activities on wetland drainage at continental
745 scale (Prigent et al., 2012). At finer scale, the variability of wetland extent
746 has also been affected by land-use change (e.g. wetland restoration,
747 deforestation, drainage for forestry, agriculture, or peat mining) and
748 consequently influences spatiotemporal patterns of CH_4 emission
749 (Petrescu et al., 2015; Zona et al., 2009). Land-use change may therefore
750 feedback water available to wetlands through altering water balance
751 between land surface and atmosphere (Woodward et al., 2014). An
752 implementation of human impacts within LSMs at large scale may be
753 important for accurate estimation of interannual variations of wetlands.
754 • *Improved modelling of soil moisture*. The quality of soil moisture
755 simulation using LSMs depends largely on the accuracy of the
756 meteorological forcing data, surface-atmosphere interaction schemes, and
757 a wide range of parameters (Zhang et al., 2013) (e.g. CO_2 concentration,
758 albedo, minimum stomatal resistance, and soil hydraulic properties). As
759 the fundamental variable for determining water table depth at global
760 scale (Fan et al., 2013), soil moisture plays a key role in simulating the
761 spatiotemporal variability of wetland dynamics. Since it is impossible to
762 produce accurate large-scale estimates of soil moisture from in situ
763 measurement networks (Bindlish et al., 2008; Dorigo et al., 2011),
764 simulation combined with long-term surface and root zone remotely
765 sensed estimates (de Rosnay et al., 2013; Kerr et al., 2010) via data
766 assimilation technology, represents a strategy to improve the capturing of
767 global wetland variability. Future hydrology-oriented satellite missions

such as Soil Moisture Active Passive (SMAP) (Entekhabi et al., 2010), and Surface Water and Ocean Topography (SWOT) mission (Durand et al., 2010) are expected to provide soil moisture and will improve the capacity of global soil moisture simulations.

- *Improved satellite benchmark observations*. Current satellite-based estimates of wetland area remain generally uncertain, despite being important for monitoring global wetland variability. Remotely sensed global inundation is prone to underestimate small wetlands, as well as covered with dense vegetation canopies (Papa et al., 2010). Moreover, estimated coastal areas show large bias due to interference with the ocean surface (Prigent et al., 2007). This raises the need for benchmark dataset useful to generate accurate products with lower uncertainties. Downscaling methodology has been made to refine existing satellite-based inundation estimates by coupling the mapping process with reliable inventories (Fluet-Chouinard et al., 2015). This may improve global inundation products, as well as the TOPMODEL parameter estimation in the future.

Conclusion

The new LPJ-wsl version incorporates a TOPMODEL approach and a permafrost module representing soil freeze-thaw processes to simulate global wetland dynamics. Once the F_{max} parameter in TOPMODEL was calibrated against a benchmark dataset, the model successfully mapped regional spatial pattern of wetlands in West Siberian Lowland and lowland Amazon basin, and captured well the spatiotemporal variations of global wetlands. The parameterization of TOPMODEL based on three DEM products, HYDRO1k, GMTED, and HydroSHEDS revealed that HydroSHEDS performed best in capturing the spatial heterogeneity and interannual variability of inundated areas compared to inventories. River-basin based parameterization schemes using HYDRO1k and GMTED marginally but significantly improve wetland area estimates. The estimates of global wetland potential/maximum is ~ 10.3 Mkm^2, with a mean annual maximum of ~ 5.17 Mkm^2 for 1980-2010. This development of the wetland modeling method reduces the uncertainties in modeling global wetland area and opens up new opportunities for studying the spatiotemporal variability of wetlands in LSMs that are directly comparable with inventories and satellite datasets.

Acknowledgement

Z. Zhang acknowledges funding by the CCES MAIOLICA2 project #42-01 and the National Natural Science Foundation of China (Y411391001). We are grateful to T. J. Bohn for providing WETCHIMP-WSL experiment results. We thank B. D. Stocker for providing HYDRO1K global river basin map. We thank T. Marthews for providing global CTI dataset of HydroSHEDS. We thank L. L. Hess for the results of dual-season inundated product of Lowland Amazon Basin.

References

Air Force Weather Agency: Data Format Handbook for AGRMET, technical report, Air Force Weather Agency's (AFWA) Agricultural Metereorological modeling system (AGRMET), Air Force Weather Agency, available at: http://www2.mmm.ucar.edu/mm5/documents/DATA_FORMAT_HANDBOOK.pdf (last access: July 2014), 2002.

Bergamaschi, P., Frankenberg, C., Meirink, J. F., Krol, M., Dentener, F., Wagner, T., Platt, U., Kaplan, J. O., Körner, S., Heimann, M., Dlugokencky, E. J., and Goede, A.: Satellite chartography of atmospheric methane from SCIAMACHY on board ENVISAT: 2. Evaluation based on inverse model simulations, Journal of Geophysical Research: Atmospheres, 112, D02304, 2007.

Beven, K. J. and Cloke, H. L.: Comment on "Hyperresolution global land surface modeling: Meeting a grand challenge for monitoring Earth's terrestrial water" by Eric F. Wood et al, Water Resources Research, 48, W01801, 2012.

Beven, K. J. and Kirkby, M. J.: A physically based, variable contributing area model of basin hydrology / Un modèle à base physique de zone d'appel variable de l'hydrologie du bassin versant, Hydrological Sciences Bulletin, 24, 43-69, 1979.

Bindlish, R., Jackson, T. J., Gasiewski, A., Stankov, B., Klein, M., Cosh, M. H., Mladenova, I., Watts, C., Vivoni, E., Lakshmi, V., Bolten, J., and Keefer, T.: Aircraft based soil moisture retrievals under mixed vegetation and topographic conditions, Remote Sensing of Environment, 112, 375-390, 2008.

Bloom, A. A., Palmer, P. I., Fraser, A., and Reay, D. S.: Seasonal variability of tropical wetland CH_4 emissions: the role of the methanogen-available carbon pool, Biogeosciences, 9, 2821-2830, 2012.

Bloom, A. A., Palmer, P. I., Fraser, A., Reay, D. S., and Frankenberg, C.: Large-Scale Controls of Methanogenesis Inferred from Methane and Gravity Spaceborne Data, Science, 327, 322-325, 2010.

Bohn, T. J., Melton, J. R., Ito, A., Kleinen, T., Spahni, R., Stocker, B. D., Zhang, B., Zhu, X., Schroeder, R., Glagolev, M. V., Maksyutov, S., Brovkin, V., Chen, G., Denisov, S. N., Eliseev, A. V., Gallego-Sala, A., McDonald, K. C., Rawlins, M. A., Riley, W. J., Subin, Z. M., Tian, H., Zhuang, Q., and Kaplan, J. O.: WETCHIMP-WSL: intercomparison of wetland methane emissions models over West Siberia, Biogeosciences, 12, 3321-3349, 2015.

Bousquet, P., Ciais, P., Miller, J. B., Dlugokencky, E. J., Hauglustaine, D. A., Prigent, C., Van der Werf, G. R., Peylin, P., Brunke, E. G., Carouge, C., Langenfelds, R. L., Lathiere, J., Papa, F., Ramonet, M., Schmidt, M., Steele, L. P., Tyler, S. C., and White, J.: Contribution of anthropogenic and natural sources to atmospheric methane variability, Nature, 443, 439-443, 2006.

Bousquet, P., Ringeval, B., Pison, I., Dlugokencky, E. J., Brunke, E. G., Carouge, C., Chevallier, F., Fortems-Cheiney, A., Frankenberg, C., Hauglustaine, D. A., Krummel, P. B., Langenfelds, R. L., Ramonet, M., Schmidt, M., Steele, L. P., Szopa, S., Yver, C., Viovy, N., and Ciais, P.: Source attribution of the changes in atmospheric methane for 2006–2008, Atmos. Chem. Phys., 11, 3689-3700, 2011.

Brown, J., Ferrians, O. J., Jr., Heginbottom J. A., and Melnikov, E. S.: Circum-arctic map of permafrost and ground ice conditions, edited by National Snow and Ice Data Center, Boulder, CO, USA, available at:

http://nsidc.org/data/docs/fgdc/ggd318_map_circumarctic/ (last access: December 2014), 2001.
Buytaert, W.: TOPMODEL, available at: http://cran.r-project.org/web/packages/topmodel/index.html, (last access: February 2015) 2015.
Chang, R. Y.-W., Miller, C. E., Dinardo, S. J., Karion, A., Sweeney, C., Daube, B. C., Henderson, J. M., Mountain, M. E., Eluszkiewicz, J., Miller, J. B., Bruhwiler, L. M. P., and Wofsy, S. C.: Methane emissions from Alaska in 2012 from CARVE airborne observations, Proceedings of the National Academy of Sciences, doi: 10.1073/pnas.1412953111, 2014. 2014.
Chen, X., Bohn, T. J., and Lettenmaier, D. P.: Model estimates of climate controls on pan-Arctic wetland methane emissions, Biogeosciences, 12, 6259-6277, 2015.
Glagolev, M., Kleptsova, I., Filippov, I., Maksyutov, S., and Machida, T.: Regional methane emission from West Siberia mire landscapes, Environmental Research Letters, 6, 045214, 2011.
Collins, W. J., Bellouin, N., Doutriaux-Boucher, M., Gedney, N., Halloran, P., Hinton, T., Hughes, J., Jones, C. D., Joshi, M., Liddicoat, S., Martin, G., O'Connor, F., Rae, J., Senior, C., Sitch, S., Totterdell, I., Wiltshire, A., and Woodward, S.: Development and evaluation of an Earth-System model – HadGEM2, Geosci. Model Dev., 4, 1051-1075, 2011.
Cosby, B. J., Hornberger, G. M., Clapp, R. B., and Ginn, T. R.: A Statistical Exploration of the Relationships of Soil Moisture Characteristics to the Physical Properties of Soils, Water Resources Research, 20, 682-690, 1984.
Danielson, J. J. and Gesch, D. B.: Global Multi-resolution Terrain Elevation Data 2010, available at http://topotools.cr.usgs.gov/gmted_viewer/ (last access: September 2014), 2011.
de Rosnay, P., Drusch, M., Vasiljevic, D., Balsamo, G., Albergel, C., and Isaksen, L.: A simplified Extended Kalman Filter for the global operational soil moisture analysis at ECMWF, Quarterly Journal of the Royal Meteorological Society, 139, 1199-1213, 2013.
Dorigo, W. A., Wagner, W., Hohensinn, R., Hahn, S., Paulik, C., Xaver, A., Gruber, A., Drusch, M., Mecklenburg, S., van Oevelen, P., Robock, A., and Jackson, T.: The International Soil Moisture Network: a data hosting facility for global in situ soil moisture measurements, Hydrol. Earth Syst. Sci., 15, 1675-1698, 2011.
Ducharne, A.: Reducing scale dependence in TOPMODEL using a dimensionless topographic index, Hydrol. Earth Syst. Sci., 13, 2399-2412, 2009.
Durand, M., Lee-Lueng, F., Lettenmaier, D. P., Alsdorf, D. E., Rodriguez, E., and Esteban-Fernandez, D.: The Surface Water and Ocean Topography Mission: Observing Terrestrial Surface Water and Oceanic Submesoscale Eddies, Proceedings of the IEEE, 98, 766-779, 2010.
Entekhabi, D., Njoku, E. G., O'Neill, P. E., Kellogg, K. H., Crow, W. T., Edelstein, W. N., Entin, J. K., Goodman, S. D., Jackson, T. J., Johnson, J., Kimball, J., Piepmeier, J. R., Koster, R. D., Martin, N., McDonald, K. C., Moghaddam, M., Moran, S., Reichle, R., Shi, J. C., Spencer, M. W., Thurman, S. W., Leung, T., and Van Zyl, J.: The Soil Moisture Active Passive (SMAP) Mission, Proceedings of the IEEE, 98, 704-716, 2010.
Fan, Y., Li, H., and Miguez-Macho, G.: Global Patterns of Groundwater Table Depth, Science, 339, 940-943, 2013.

907 Fan, Y. and Miguez-Macho, G.: A simple hydrologic framework for simulating
908 wetlands in climate and earth system models, Clim Dyn, 37, 253-278, 2011.
909 Fisher, R. E., Sriskantharajah, S., Lowry, D., Lanoisellé, M., Fowler, C. M. R., James,
910 R. H., Hermansen, O., Lund Myhre, C., Stohl, A., Greinert, J., Nisbet-Jones, P. B. R.,
911 Mienert, J., and Nisbet, E. G.: Arctic methane sources: Isotopic evidence for
912 atmospheric inputs, Geophysical Research Letters, 38, L21803, 2011.
913 Fluet-Chouinard, E., Lehner, B., Rebelo, L.-M., Papa, F., and Hamilton, S. K.:
914 Development of a global inundation map at high spatial resolution from
915 topographic downscaling of coarse-scale remote sensing data, Remote Sensing of
916 Environment, 158, 348-361, 2015.
917 Gedney, N. and Cox, P. M.: The Sensitivity of Global Climate Model Simulations to
918 the Representation of Soil Moisture Heterogeneity, Journal of Hydrometeorology,
919 4, 1265-1275, 2003.
920 Gerten, D., Schaphoff, S., Haberlandt, U., Lucht, W., and Sitch, S.: Terrestrial
921 vegetation and water balance—hydrological evaluation of a dynamic global
922 vegetation model, Journal of Hydrology, 286, 249-270, 2004.
923 Glagolev, M., Kleptsova, I., Filippov, I., Maksyutov, S., and Machida, T.: Regional
924 methane emission from West Siberia mire landscapes, Environmental Research
925 Letters, 6, 045214, 2011.
926 Grabs, T., Seibert, J., Bishop, K., and Laudon, H.: Modeling spatial patterns of
927 saturated areas: A comparison of the topographic wetness index and a dynamic
928 distributed model, Journal of Hydrology, 373, 15-23, 2009.
929 Gurney, K. R., Law, R. M., Denning, A. S., Rayner, P. J., Baker, D., Bousquet, P.,
930 Bruhwiler, L., Chen, Y.-H., Ciais, P., Fan, S., Fung, I. Y., Gloor, M., Heimann, M.,
931 Higuchi, K. A. Z., John, J., Kowalczyk, E. V. A., Maki, T., Maksyutov, S., Peylin, P.,
932 Prather, M., Pak, B. C., Sarmiento, J., Taguchi, S., Takahashi, T., and Yuen, C.-W.:
933 TransCom 3 CO_2 inversion intercomparison: 1. Annual mean control results and
934 sensitivity to transport and prior flux information, Tellus B, 55, 555-579, 2003.
935 Güntner, A., Seibert, J., and Uhlenbrook, S.: Modeling spatial patterns of saturated
936 areas: An evaluation of different terrain indices, Water Resources Research, 40,
937 W05114, 2004.
938 Harris, I., Jones, P. D., Osborn, T. J., and Lister, D. H.: Updated high-resolution
939 grids of monthly climatic observations – the CRU TS3.10 Dataset, International
940 Journal of Climatology, 34, 623-642, 2014.
941 Hess, L., Melack, J., Affonso, A., Barbosa, C., Gastil-Buhl, M., and Novo, E. L. M.:
942 Wetlands of the Lowland Amazon Basin: Extent, Vegetative Cover, and Dual-
943 season Inundated Area as Mapped with JERS-1 Synthetic Aperture Radar,
944 Wetlands, doi: 10.1007/s13157-015-0666-y, 2015. 1-12, 2015.
945 Hodson, E. L., Poulter, B., Zimmermann, N. E., Prigent, C., and Kaplan, J. O.: The El
946 Niño–Southern Oscillation and wetland methane interannual variability,
947 Geophysical Research Letters, 38, L08810, 2011.
948 IPCC: Climate Change 2013: The Physical Science Basis. Contribution of Working
949 Group I to the Fifth Assessment Report of the Intergovernmental Panel on
950 Climate Change, Cambridge University Press, Cambridge, United Kingdom and
951 New York, NY, USA, 2013.
952 Ito, A. and Inatomi, M.: Use of a process-based model for assessing the methane
953 budgets of global terrestrial ecosystems and evaluation of uncertainty,
954 Biogeosciences, 9, 759-773, 2012.

955 Jennifer, D. W., John, S. K., Annett, B., and Kyle, C. M.: Surface water inundation in
956 the boreal-Arctic: potential impacts on regional methane emissions,
957 Environmental Research Letters, 9, 075001, 2014.
958 Junk, W., Piedade, M., Schöngart, J., Cohn-Haft, M., Adeney, J. M., and Wittmann, F.:
959 A Classification of Major Naturally-Occurring Amazonian Lowland Wetlands,
960 Wetlands, 31, 623-640, 2011.
961 Kaplan, J. O.: Wetlands at the Last Glacial Maximum: Distribution and methane
962 emissions, Geophysical Research Letters, 29, 3-1-3-4, 2002.
963 Kerr, Y. H., Waldteufel, P., Wigneron, J. P., Delwart, S., Cabot, F., Boutin, J.,
964 Escorihuela, M. J., Font, J., Reul, N., Gruhier, C., Juglea, S. E., Drinkwater, M. R.,
965 Hahne, A., Martin-Neira, M., and Mecklenburg, S.: The SMOS Mission: New Tool
966 for Monitoring Key Elements ofthe Global Water Cycle, Proceedings of the IEEE,
967 98, 666-687, 2010.
968 Kim, Y., Kimball, J. S., Zhang, K., and McDonald, K. C.: Satellite detection of
969 increasing Northern Hemisphere non-frozen seasons from 1979 to 2008:
970 Implications for regional vegetation growth, Remote Sensing of Environment,
971 121, 472-487, 2012.
972 Kirschke, S., Bousquet, P., Ciais, P., Saunois, M., Canadell, J. G., Dlugokencky, E. J.,
973 Bergamaschi, P., Bergmann, D., Blake, D. R., Bruhwiler, L., Cameron-Smith, P.,
974 Castaldi, S., Chevallier, F., Feng, L., Fraser, A., Heimann, M., Hodson, E. L.,
975 Houweling, S., Josse, B., Fraser, P. J., Krummel, P. B., Lamarque, J.-F., Langenfelds,
976 R. L., Le Quere, C., Naik, V., O'Doherty, S., Palmer, P. I., Pison, I., Plummer, D.,
977 Poulter, B., Prinn, R. G., Rigby, M., Ringeval, B., Santini, M., Schmidt, M., Shindell,
978 D. T., Simpson, I. J., Spahni, R., Steele, L. P., Strode, S. A., Sudo, K., Szopa, S., van der
979 Werf, G. R., Voulgarakis, A., van Weele, M., Weiss, R. F., Williams, J. E., and Zeng,
980 G.: Three decades of global methane sources and sinks, Nature Geosci, 6, 813-
981 823, 2013.
982 Kleinen, T., Brovkin, V., and Schuldt, R. J.: A dynamic model of wetland extent and
983 peat accumulation: results for the Holocene, Biogeosciences, 9, 235-248, 2012.
984 Kopecký, M. and Čížková, Š.: Using topographic wetness index in vegetation
985 ecology: does the algorithm matter?, Applied Vegetation Science, 13, 450-459,
986 2010.
987 Kopecký, M. and Čížková, Š.: Using topographic wetness index in vegetation
988 ecology: does the algorithm matter?, Applied Vegetation Science, 13, 450-459,
989 2010.
990 Leff, B., Ramankutty, N., and Foley, J. A.: Geographic distribution of major crops
991 across the world, Global Biogeochemical Cycles, 18, GB1009, 2004.
992 Lehner, B. and Döll, P.: Development and validation of a global database of lakes,
993 reservoirs and wetlands, Journal of Hydrology, 296, 1-22, 2004.
994 Lehner, B. and Grill, G.: Global river hydrography and network routing: baseline
995 data and new approaches to study the world's large river systems, Hydrological
996 Processes, 27, 2171-2186, 2013.
997 Lehner, B., Verdin, K., and Jarvis, A.: New Global Hydrography Derived From
998 Spaceborne Elevation Data, Eos, Transactions American Geophysical Union, 89,
999 93-94, 2008.
1000 Lei, H., Huang, M., Leung, L. R., Yang, D., Shi, X., Mao, J., Hayes, D. J., Schwalm, C. R.,
1001 Wei, Y., and Liu, S.: Sensitivity of global terrestrial gross primary production to
1002 hydrologic states simulated by the Community Land Model using two runoff

1003 parameterizations, Journal of Advances in Modeling Earth Systems, 6, 658-679,
1004 2014.
1005 Liang, X., Lettenmaier, D. P., Wood, E. F., and Burges, S. J.: A simple hydrologically
1006 based model of land surface water and energy fluxes for general circulation
1007 models, Journal of Geophysical Research: Atmospheres, 99, 14415-14428, 1994.
1008 Lin, K., Zhang, Q., and Chen, X.: An evaluation of impacts of DEM resolution and
1009 parameter correlation on TOPMODEL modeling uncertainty, Journal of
1010 Hydrology, 394, 370-383, 2010.
1011 Lin, S., Jing, C., Coles, N., Chaplot, V., Moore, N., and Wu, J.: Evaluating DEM source
1012 and resolution uncertainties in the Soil and Water Assessment Tool, Stoch
1013 Environ Res Risk Assess, 27, 209-221, 2013.
1014 Marthews, T. R., Dadson, S. J., Lehner, B., Abele, S., and Gedney, N.: High-
1015 resolution global topographic index values for use in large-scale hydrological
1016 modelling, Hydrol. Earth Syst. Sci., 19, 91-104, 2015.
1017 Marthews, T. R., Quesada, C. A., Galbraith, D. R., Malhi, Y., Mullins, C. E., Hodnett,
1018 M. G., and Dharssi, I.: High-resolution hydraulic parameter maps for surface soils
1019 in tropical South America, Geosci. Model Dev., 7, 711-723, 2014.
1020 Matthews, E. and Fung, I.: Methane emission from natural wetlands: Global
1021 distribution, area, and environmental characteristics of sources, Global
1022 Biogeochemical Cycles, 1, 61-86, 1987.
1023 Melack, J. M., Hess, L. L., Gastil, M., Forsberg, B. R., Hamilton, S. K., Lima, I. B. T.,
1024 and Novo, E. M. L. M.: Regionalization of methane emissions in the Amazon Basin
1025 with microwave remote sensing, Global Change Biology, 10, 530-544, 2004.
1026 Melton, J. R., Wania, R., Hodson, E. L., Poulter, B., Ringeval, B., Spahni, R., Bohn, T.,
1027 Avis, C. A., Beerling, D. J., Chen, G., Eliseev, A. V., Denisov, S. N., Hopcroft, P. O.,
1028 Lettenmaier, D. P., Riley, W. J., Singarayer, J. S., Subin, Z. M., Tian, H., Zürcher, S.,
1029 Brovkin, V., van Bodegom, P. M., Kleinen, T., Yu, Z. C., and Kaplan, J. O.: Present
1030 state of global wetland extent and wetland methane modelling: conclusions from
1031 a model inter-comparison project (WETCHIMP), Biogeosciences, 10, 753-788,
1032 2013.
1033 Meng, L., Hess, P. G. M., Mahowald, N. M., Yavitt, J. B., Riley, W. J., Subin, Z. M.,
1034 Lawrence, D. M., Swenson, S. C., Jauhiainen, J., and Fuka, D. R.: Sensitivity of
1035 wetland methane emissions to model assumptions: application and model
1036 testing against site observations, Biogeosciences, 9, 2793-2819, 2012.
1037 Mulligan, M. and Wainwright, J.: Modelling and Model Building, in:
1038 Environmental Modelling, John Wiley & Sons, Ltd, Chichester, UK, 7-26, 2013.
1039 Nachtergaele, F., Van Velthuizen, H., Verelst, L., Batjes, N., Dijkshoorn, K., Van
1040 Engelen, V., Fischer, G., Jones, A., Montanarella, L., and Petri, M.: Harmonized
1041 world soil database, FAO, Rome, Italy and IIASA, Laxenburg, Austria, 2008.
1042 Nisbet, E. G., Dlugokencky, E. J., and Bousquet, P.: Methane on the Rise—Again,
1043 Science, 343, 493-495, 2014.
1044 National Wetland Working Group: Wetlands of Canada. Ecolgoical Land
1045 Classification Series, No., 24. Canada Committee on Ecological Land
1046 Classification, Sustainable Development Branch, Environment Canada and
1047 Polyscience Publications Inc, Montreal, Quebec, Canada.
1048 Niu, G.-Y., Yang, Z.-L., Dickinson, R. E., and Gulden, L. E.: A simple TOPMODEL-
1049 based runoff parameterization (SIMTOP) for use in global climate models,
1050 Journal of Geophysical Research: Atmospheres, 110, D21106, 2005.

Pan, F., Peters-Lidard, C. D., Sale, M. J., and King, A. W.: A comparison of geographical information systems–based algorithms for computing the TOPMODEL topographic index, Water Resources Research, 40, W06303, 2004.
Papa, F., Prigent, C., Aires, F., Jimenez, C., Rossow, W. B., and Matthews, E.: Interannual variability of surface water extent at the global scale, 1993–2004, Journal of Geophysical Research: Atmospheres, 115, D12111, 2010.
Peregon, A., Maksyutov, S., Kosykh, N. P., and Mironycheva-Tokareva, N. P.: Map-based inventory of wetland biomass and net primary production in western Siberia, Journal of Geophysical Research: Biogeosciences, 113, G01007, 2008.
Petrescu, A. M. R., Lohila, A., Tuovinen, J.-P., Baldocchi, D. D., Desai, A. R., Roulet, N. T., Vesala, T., Dolman, A. J., Oechel, W. C., Marcolla, B., Friborg, T., Rinne, J., Matthes, J. H., Merbold, L., Meijide, A., Kiely, G., Sottocornola, M., Sachs, T., Zona, D., Varlagin, A., Lai, D. Y. F., Veenendaal, E., Parmentier, F.-J. W., Skiba, U., Lund, M., Hensen, A., van Huissteden, J., Flanagan, L. B., Shurpali, N. J., Grünwald, T., Humphreys, E. R., Jackowicz-Korczyński, M., Aurela, M. A., Laurila, T., Grüning, C., Corradi, C. A. R., Schrier-Uijl, A. P., Christensen, T. R., Tamstorf, M. P., Mastepanov, M., Martikainen, P. J., Verma, S. B., Bernhofer, C., and Cescatti, A.: The uncertain climate footprint of wetlands under human pressure, Proceedings of the National Academy of Sciences, 112, 4594-4599, 2015.
Petrescu, A. M. R., van Beek, L. P. H., van Huissteden, J., Prigent, C., Sachs, T., Corradi, C. A. R., Parmentier, F. J. W., and Dolman, A. J.: Modeling regional to global CH_4 emissions of boreal and arctic wetlands, Global Biogeochemical Cycles, 24, GB4009, 2010.
Poulter, B., Ciais, P., Hodson, E., Lischke, H., Maignan, F., Plummer, S., and Zimmermann, N. E.: Plant functional type mapping for earth system models, Geosci. Model Dev., 4, 993-1010, 2011.
Poulter, B., Bousquet, P., Canadell, P., Ciais, P., Peregon, A., Arora, V., Beerling, D., Brovkin, V., Hopcroft, P., Jones, C., Joos, F., Gedney, N., Ito, A., Kleinen, T., Koven, C., MacDonald, K., Melton, J., Peng, C., Peng, S., Schroder, R., Prigent, C., Riley, B., Saito, M., Spahni, R., Tian, H., Taylor, L., Viovy, N., Wilton, D., Wiltshire, A., Xu, X., and Zhang, Z.,: Global wetland contribution to increasing atmospheric methane concentrations (2000-2012), in preparation, 2015.
Prigent, C., Papa, F., Aires, F., Jimenez, C., Rossow, W. B., and Matthews, E.: Changes in land surface water dynamics since the 1990s and relation to population pressure, Geophysical Research Letters, 39, L08403, 2012.
Prigent, C., Papa, F., Aires, F., Rossow, W. B., and Matthews, E.: Global inundation dynamics inferred from multiple satellite observations, 1993–2000, Journal of Geophysical Research: Atmospheres, 112, D12107, 2007.
Quinn, P. F., Beven, K. J., and Lamb, R.: The in(a/tan/β) index: How to calculate it and how to use it within the topmodel framework, Hydrological Processes, 9, 161-182, 1995.
Quiquet, A., Archibald, A. T., Friend, A. D., Chappellaz, J., Levine, J. G., Stone, E. J., Telford, P. J., and Pyle, J. A.: The relative importance of methane sources and sinks over the Last Interglacial period and into the last glaciation, Quaternary Science Reviews, 112, 1-16, 2015.
Ringeval, B., Decharme, B., Piao, S. L., Ciais, P., Papa, F., de Noblet-Ducoudré, N., Prigent, C., Friedlingstein, P., Gouttevin, I., Koven, C., and Ducharne, A.: Modelling sub-grid wetland in the ORCHIDEE global land surface model: evaluation against river discharges and remotely sensed data, Geosci. Model Dev., 5, 941-962, 2012.

Ringeval, B., Houweling, S., van Bodegom, P. M., Spahni, R., van Beek, R., Joos, F., and Röckmann, T.: Methane emissions from floodplains in the Amazon Basin: challenges in developing a process-based model for global applications, Biogeosciences, 11, 1519-1558, 2014.
Rinne, J., Riutta, T., Pihlatie, M., Aurela, M., Haapanala, S., Tuovinen, J.-P., Tuittila, E.-S., and Vesala, T.: Annual cycle of methane emission from a boreal fen measured by the eddy covariance technique, Tellus B, 59, 449-457, 2007.
Seneviratne, S. I., Corti, T., Davin, E. L., Hirschi, M., Jaeger, E. B., Lehner, I., Orlowsky, B., and Teuling, A. J.: Investigating soil moisture–climate interactions in a changing climate: A review, Earth-Science Reviews, 99, 125-161, 2010.
Sheng, Y., Smith, L. C., MacDonald, G. M., Kremenetski, K. V., Frey, K. E., Velichko, A. A., Lee, M., Beilman, D. W., and Dubinin, P.: A high-resolution GIS-based inventory of the west Siberian peat carbon pool, Global Biogeochemical Cycles, 18, GB3004, 2004.
Singarayer, J. S., Valdes, P. J., Friedlingstein, P., Nelson, S., and Beerling, D. J.: Late Holocene methane rise caused by orbitally controlled increase in tropical sources, Nature, 470, 82-85, 2011.
Sitch, S., Smith, B., Prentice, I. C., Arneth, A., Bondeau, A., Cramer, W., Kaplan, J. O., Levis, S., Lucht, W., Sykes, M. T., Thonicke, K., and Venevsky, S.: Evaluation of ecosystem dynamics, plant geography and terrestrial carbon cycling in the LPJ dynamic global vegetation model, Global Change Biology, 9, 161-185, 2003.
Sivapalan, M., Beven, K., and Wood, E. F.: On hydrologic similarity: 2. A scaled model of storm runoff production, Water Resources Research, 23, 2266-2278, 1987.
Sørensen, R. and Seibert, J.: Effects of DEM resolution on the calculation of topographical indices: TWI and its components, Journal of Hydrology, 347, 79-89, 2007.
Spahni, R., Wania, R., Neef, L., van Weele, M., Pison, I., Bousquet, P., Frankenberg, C., Foster, P. N., Joos, F., Prentice, I. C., and van Velthoven, P.: Constraining global methane emissions and uptake by ecosystems, Biogeosciences, 8, 1643-1665, 2011.
Stieglitz, M., Rind, D., Famiglietti, J., and Rosenzweig, C.: An Efficient Approach to Modeling the Topographic Control of Surface Hydrology for Regional and Global Climate Modeling, Journal of Climate, 10, 118-137, 1997.
Stocker, B. D., Roth, R., Joos, F., Spahni, R., Steinacher, M., Zaehle, S., Bouwman, L., Xu, R., and Prentice, I. C.: Multiple greenhouse-gas feedbacks from the land biosphere under future climate change scenarios, Nature Clim. Change, 3, 666-672, 2013.
Stocker, B. D., Spahni, R., and Joos, F.: DYPTOP: a cost-efficient TOPMODEL implementation to simulate sub-grid spatio-temporal dynamics of global wetlands and peatlands, Geosci. Model Dev., 7, 3089-3110, 2014.
Tarnocai, C., Canadell, J. G., Schuur, E. A. G., Kuhry, P., Mazhitova, G., and Zimov, S.: Soil organic carbon pools in the northern circumpolar permafrost region, Global Biogeochemical Cycles, 23, GB2023, 2009.
Turetsky, M. R., Kotowska, A., Bubier, J., Dise, N. B., Crill, P., Hornibrook, E. R. C., Minkkinen, K., Moore, T. R., Myers-Smith, I. H., Nykänen, H., Olefeldt, D., Rinne, J., Saarnio, S., Shurpali, N., Tuittila, E.-S., Waddington, J. M., White, J. R., Wickland, K. P., and Wilmking, M.: A synthesis of methane emissions from 71 northern,

temperate, and subtropical wetlands, Global Change Biology, 20, 2183-2197, 2014.
USGS: HYDRO1k Elevation Derivative Database, US Geological Survey Earth Resources Observation and Science (EROS) Data Center (EDC), Sioux Falls, South Dakota, USA, 1996.
Verpoorter, C., Kutser, T., Seekell, D. A., and Tranvik, L. J.: A global inventory of lakes based on high-resolution satellite imagery, Geophysical Research Letters, 41, 6396-6402, 2014.
Wania, R., Melton, J. R., Hodson, E. L., Poulter, B., Ringeval, B., Spahni, R., Bohn, T., Avis, C. A., Chen, G., Eliseev, A. V., Hopcroft, P. O., Riley, W. J., Subin, Z. M., Tian, H., van Bodegom, P. M., Kleinen, T., Yu, Z. C., Singarayer, J. S., Zürcher, S., Lettenmaier, D. P., Beerling, D. J., Denisov, S. N., Prigent, C., Papa, F., and Kaplan, J. O.: Present state of global wetland extent and wetland methane modelling: methodology of a model inter-comparison project (WETCHIMP), Geosci. Model Dev., 6, 617-641, 2013.
Wania, R., Ross, I., and Prentice, I. C.: Integrating peatlands and permafrost into a dynamic global vegetation model: 1. Evaluation and sensitivity of physical land surface processes, Global Biogeochemical Cycles, 23, GB3014, 2009.
Ward, R. C. and Robinson, M.: Principles of Hydrology, 4th Edn, McGraw-Hill, Maidenhead, UK, 2000.
Whalen, S. C. and Reeburgh, W. S.: Interannual variations in tundra methane emission: A 4-year time series at fixed sites, Global Biogeochemical Cycles, 6, 139-159, 1992.
Wilson, J. P. and Gallant, J. C.: Terrain analysis: principles and applications, John Wiley & Sons, New York, NY, USA, 2000.
Wood, E. F., Roundy, J. K., Troy, T. J., van Beek, L. P. H., Bierkens, M. F. P., Blyth, E., de Roo, A., Döll, P., Ek, M., Famiglietti, J., Gochis, D., van de Giesen, N., Houser, P., Jaffé, P. R., Kollet, S., Lehner, B., Lettenmaier, D. P., Peters-Lidard, C., Sivapalan, M., Sheffield, J., Wade, A., and Whitehead, P.: Hyperresolution global land surface modeling: Meeting a grand challenge for monitoring Earth's terrestrial water, Water Resources Research, 47, W05301, 2011.
Woodward, C., Shulmeister, J., Larsen, J., Jacobsen, G. E., and Zawadzki, A.: The hydrological legacy of deforestation on global wetlands, Science, 346, 844-847, 2014.
Zhang, Z., Jiang, H., Liu, J., Ju, W., and Zhang, X.: Effect of heterogeneous atmospheric CO_2 on simulated global carbon budget, Global and Planetary Change, 101, 33-51, 2013.
Zhu, X., Zhuang, Q., Lu, X., and Song, L.: Spatial scale-dependent land–atmospheric methane exchanges in the northern high latitudes from 1993 to 2004, Biogeosciences, 11, 1693-1704, 2014.
Zhuang, Q., Melillo, J. M., Kicklighter, D. W., Prinn, R. G., McGuire, A. D., Steudler, P. A., Felzer, B. S., and Hu, S.: Methane fluxes between terrestrial ecosystems and the atmosphere at northern high latitudes during the past century: A retrospective analysis with a process-based biogeochemistry model, Global Biogeochemical Cycles, 18, GB3010, 2004.
Zona, D., Oechel, W. C., Kochendorfer, J., Paw U, K. T., Salyuk, A. N., Olivas, P. C., Oberbauer, S. F., and Lipson, D. A.: Methane fluxes during the initiation of a large-scale water table manipulation experiment in the Alaskan Arctic tundra, Global Biogeochemical Cycles, 23, GB2013, 2009.

1197 Zürcher, S., Spahni, R., Joos, F., Steinacher, M., and Fischer, H.: Impact of an abrupt
1198 cooling event on interglacial methane emissions in northern peatlands,
1199 Biogeosciences, 10, 1963-1981, 2013.

Tables

Table 1. Soil parameters for LPJ-wsl soil classes. f is a parameter describing the exponential decline of transmissivity with depth for each soil type.

Soil type	*f*	Mineral Content (%)	Organic Content (%)	Wilting Point (%)	Porosity (%)
Clay Heavy	3.2	0.508	0.01	0.138	0.138
Silty Clay	3.1	0.531	0.01	0.126	0.468
Clay	2.8	0.531	0.01	0.138	0.468
Silty Clay Loam	2.9	0.534	0.01	0.120	0.464
Clay Loam	2.7	0.595	0.01	0.103	0.465
Silt	3.4	0.593	0.01	0.084	0.476
Silt Loam	2.6	0.593	0.01	0.084	0.476
Sandy Clay	2.5	0.535	0.01	0.100	0.406
Loam	2.5	0.535	0.01	0.066	0.439
Sandy Clay Loam	2.4	0.565	0.01	0.067	0.404
Sandy Loam	2.3	0.565	0.01	0.047	0.434
Loamy Sand	2.2	0.578	0.01	0.028	0.421
Sand	2.1	0.578	0.01	0.010	0.339
Organic	2.5	0.01	0.20	0.066	0.439

Table 2 Model experiments for different parameterization schemes and corresponding DEM products applied in this study.

Model Experiment	DEM	DEM source	Resolution (arc seconds)	Coverage	River Basin	Aggregation type	Hydro-corrected
HYDRO1k_BASIN	Hydro1k	GTOPO30	30	Global*	HYDRO1K	Catchment	Yes
HYDRO1k_GRID	Hydro1k	GTOPO30	30	Global*	HYDRO1K	Grid	Yes
GMTED_BASIN	GMTED	SRTM&others	15	Global	HYDRO1K	Catchment	No
GMTED_GRID	GMTED	SRTM&others	15	Global	HYDRO1K	Grid	No
SHEDS_BASIN	HydroSHEDS	SRTM	15	<60°N	HydroSHEDS	Catchment	Yes
SHEDS_GRID	HydroSHEDS	SRTM	15	<60°N	HydroSHEDS	Grid	Yes

Table 3 Summary of simulated and observed mean annual minimum (MIN), maximum (MAX), and amplitude (AMP) of wetland extent for 1980-2010. All units are Mkm^2 (106 km^2) ± 1σ, where standard deviation represents the inter-annual variation in model estimates except for the row Average, which represents uncertainties of estimates from each model experiment.

Model	Lowland Amazon Basin			West Siberian Lowland			Global		
	MIN	MAX	AMP	MIN	MAX	AMP	MIN	MAX	AMP
SHEDS_BASIN	0.27±0.02	0.38±0.01	0.11±0.01	0±0	0.45±0.05	0.45±0.05	2.96±0.06	5.17±0.11	2.23±0.10
SHEDS_GRID	0.32±0.01	0.40±0.01	0.08±0.01	0±0	0.45±0.05	0.45±0.05	3.56±0.06	5.93±0.11	2.38±0.10
GMTED_BASIN	0.21±0.02	0.35±0.01	0.14±0.02	0±0	0.39±0.06	0.39±0.06	2.09±0.05	3.75±0.12	1.66±0.12
GMTED_GRID	0.19±0.02	0.34 ±0.01	0.15±0.02	0±0	0.38±0.06	0.38±0.06	1.80±0.05	3.32±0.13	1.52±0.13
HYDRO1k_BASIN	0.25±0.02	0.37±0.01	0.12±0.01	0±0	0.39±0.06	0.39±0.06	2.44±0.05	4.32±0.11	1.89±0.11
HYDRO1k_GRID	0.22±0.02	0.36±0.01	0.14±0.02	0±0	0.36±0.07	0.36±0.07	2.12±0.05	3.73±0.13	1.61±0.13
Average	**0.27±0.04**	**0.38±0.02**	**0.11±0.01**	**0±0**	**0.40±0.04**	**0.40±0.04**	**2.49±0.65**	**4.37±0.99**	**1.88±0.35**
Observations									
Hess2015	0.23	0.58							
GIEMS	0.12±0.01	0.25±0.03	0.14±0.04	0±0	0.24±0.05	0.25±0.05	1.38±0.09	4.47±0.20	3.09±0.19
SWAMPS-GLWD	0.22±0.03	0.34±0.01	0.12±0.03	0±0	0.50±0.03	0.51±0.03	3.03±0.13	6.62±0.18	3.63±0.14

Table 4 Spearman correlations between satellite-based vs. modeled interannual anomalies of the grid-cells contained in each region defined in Fig. 2f at global scale. Values out and in parentheses are correlation efficient with SWAMPS-GLWD and GIEMS respectively. The two highest value within one column is in bold.

Regions	SHDES BASIN	SHDES GRID	GMTED BASIN	GMTED GRID	HYDRO1K BASIN	HYDRO1k GRID
Boreal North America	**0.770**	**0.768**	0.751	0.745	0.765	0.748
	(**0.378**)	(0.376)	(0.354)	(0.341)	**(0.378)**	(0.343)
Boreal Eurasia	**0.785**	**0.782**	0.763	0.764	0.763	0.760
	(**0.513**)	**(0.511)**	(0.487)	(0.487)	(0.493)	(0.484)
Europe	0.**604**	**0.595**	0.313	0.211	0.588	0.218
	(0.091)	(0.079)	(-0.198)	(**-0.278**)	(0.076)	**(-0.272)**
Tropical South America	0.723	**0.725**	0.724	0.666	0.708	**0.726**
	(**0.838**)	(0.831)	(0.835)	(0.825)	**(0.836)**	(0.835)
South Africa	0.082	0.044	**0.084**	0.076	0.040	**0.088**
	(0.736)	(0.725)	(0.735)	(0.734)	(0.717)	(**0.740**)
Tropical Asia	**0.689**	**0.681**	0.705	0.677	0.670	0.648
	(0.674)	(0.673)	(**0.682**)	(0.625)	(0.660)	(0.632)
Temperate North America	0.359	0.380	0.406	0.347	**0.518**	**0.479**
	(0.139)	(0.155)	(0.262)	(0.229)	**(0.288)**	(**0.305**)
Temperate South America	**-0.193**	**-0.205**	-0.153	-0.162	-0.178	-0.166
	(0.633)	(0.597)	(0.622)	(**0.641**)	(0.627)	(0.627)
Temperate Eurasia	**0.742**	**0.760**	0.735	0.721	0.732	0.716
	(0.645)	(**0.660**)	(0.642)	(0.643)	(0.642)	(0.642

Table 5. List of global and regional wetland CH_4 estimates from our model experiments (see Table 2) over the period 1980-2000. All units are Tg CH_4 yr^{-1}±1σ, where standard deviation represents the interannual variation in the model estimates. Note that estimates from some reference studies are not for the same period.

Estimates	Global	Regions			Hotspot			
		Tropics (20N-30S)	Temperate (20-45N, 30S-50S)	Northern (>45N)	Central Amazon[b]	WSL	Hudson Bay	Alaska
SHEDS_BASIN	171.9	109.3±2.3	26.4±1.0	36.1±1.8	10.9±0.3	5.4±0.9	6.5±0.5	1.7±0.3
SHEDS_GRID	193.0	123.7±2.2	31.4±1.0	38.7±1.9	11.4±0.3	5.5±0.9	7.1±0.6	1.5±0.3
GMTED_BASIN	130.1	85.5±2.3	19.0±0.9	26.3±1.4	9.5±0.4	4.5±0.9	4.4±0.6	1.6±0.3
GMTED_GRID	117.2	76.7±2.3	16.4±0.9	24.2±1.4	9.2±0.4	4.1±0.9	4.2±0.6	1.4±0.3
HYDRO1K_BASIN	148.3	96.4±2.3	21.5±0.9	30.3±1.6	10.4±0.3	4.4±0.9	5.8±0.6	1.7±0.3
HYDRO1K_GRID	128.8	85.0±2.3	17.8±0.9	26.0±1.4	10.0±0.4	3.9±0.9	4.8±0.6	1.5±0.3
Melton et al. (2013)[a]	190±39						5.4±3.2	
Zhu et al. (2015)	209-245			38.1-55.4				
Chen et al. (2015)				35			3.11±0.45	
Zhu et al. (2014)				34-58			3.1± 0.5	
Ringeval et al. (2012)	193.8	102	51	40.8				
Glagolev et al. (2011)						3.91±1.3		
Melack et al. (2004)					9.1			
Zhuang et al. (2004)				57.3				
Chang et al. (2014)								2.1±0.5
Bloom et al. (2012)		111.1						
Bousquet et al. (2011)	151±10	91±11						
Bloom et al. (2010)	165±50	91±28					4.9±1.4	

[a] WETCHIMP estimates for 1993-2004

[b] Central Amazon (54-72°W,0-8°S)

Figures

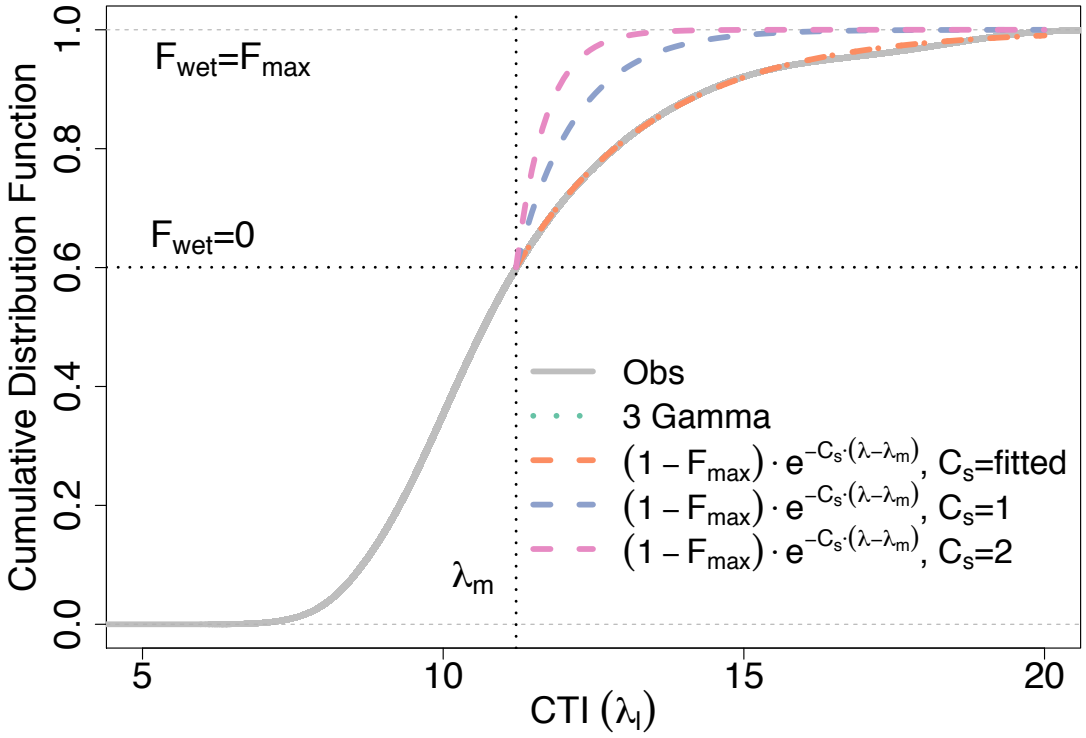

Figure 1. Cumulative distribution function (CDF) of the fitted exponential curve (blue line) as a function of compound topographic index (CTI) in comparison with the three-parameter gamma function (red line), as well as the observations (grey line) with in a sample grid box.

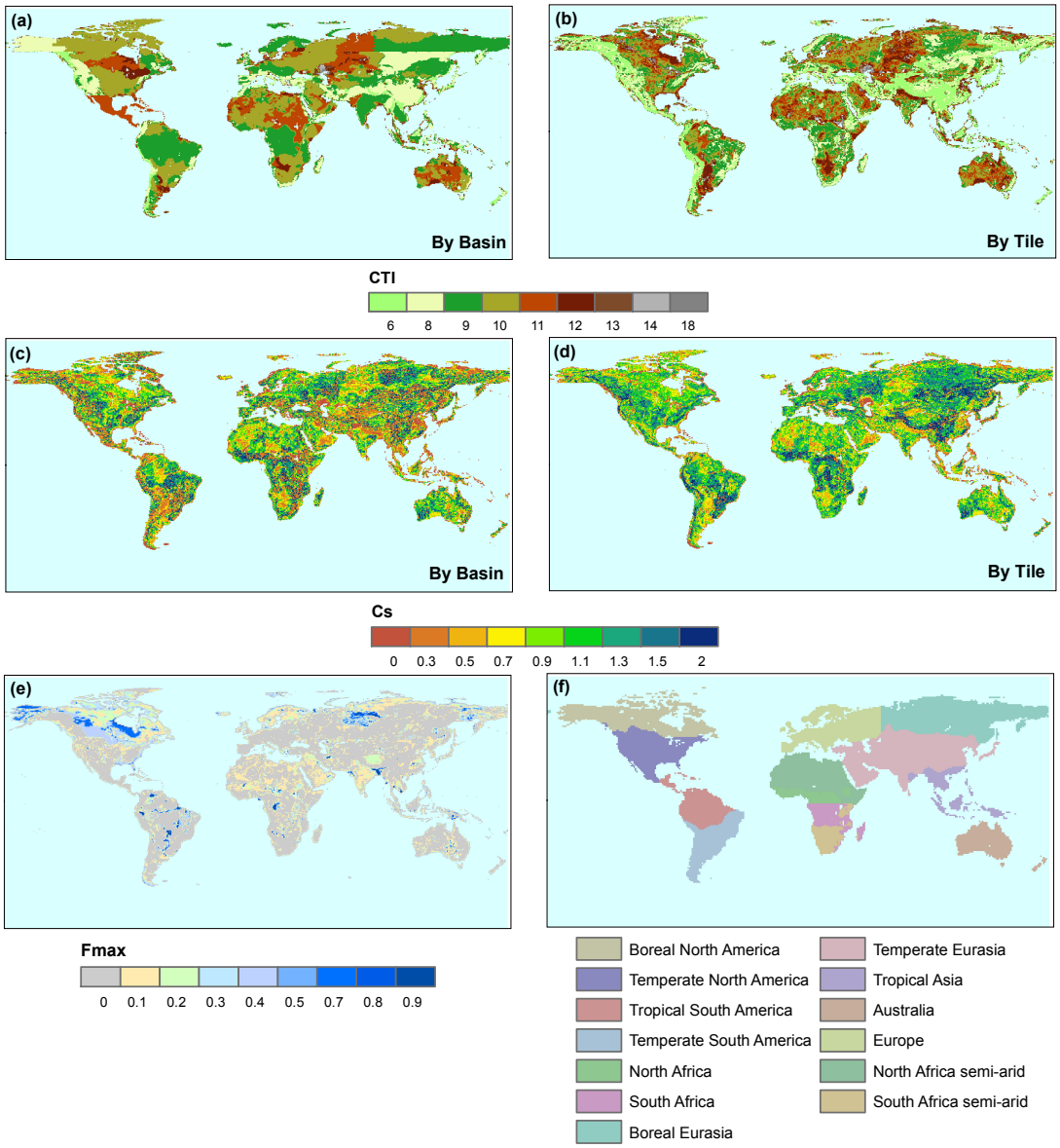

Figure 2. TOPMODEL parameter maps in model experiments. Mean CTI (a, b) and C_s (c, d) aggregated by river basin (denoted as "By Basin") and grid cell (denoted as "By Tile") schemes from HydroSHEDS were listed. F_{max} (e) for calibration was generated using SWAMPS-GLWD and GLWD. Map of regions (f) was used to partition globe into boreal, temperate, tropical biomes (Gurney et al. 2003).

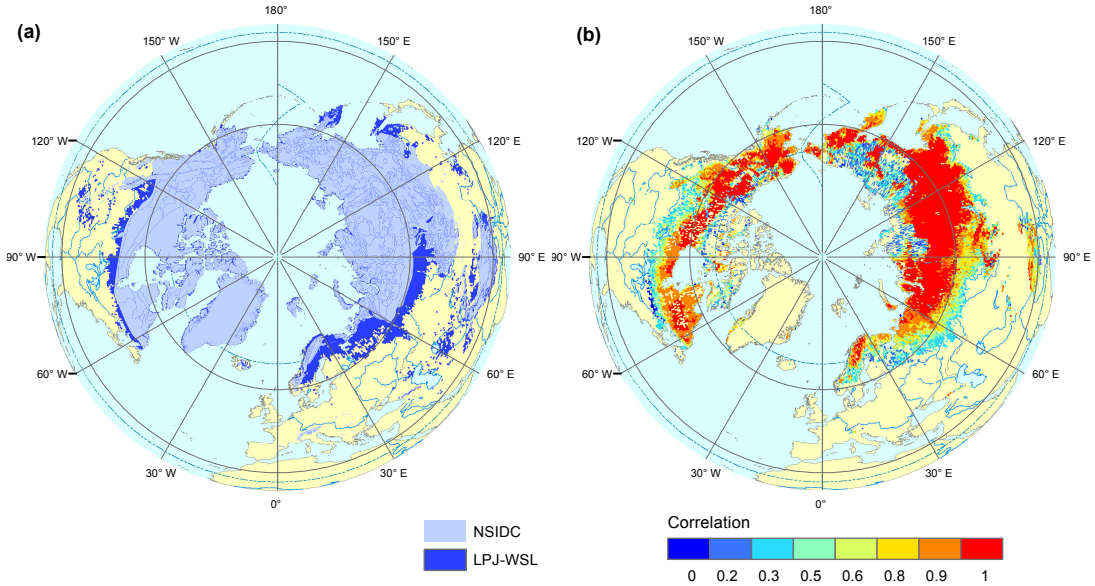

Figure 3 Evaluation of permafrost simulation in LPJ-wsl. (a) Inventory-based (light blue) and simulated (dark blue) permafrost extent from NSIDC and LPJ-wsl respectively. The inventory contains discontinuous, sporadic or isolated permafrost boundaries, as well as the location of subsea and relict permafrost. We only compare the distribution of all permafrost against model outputs without distinguishing each permafrost types. (b) Spatial distribution of Spearman correlation between simulated monthly frozen-days from LPJ-wsl over 2002-2011 and satellite retrievals of FT status from AMSR-E.

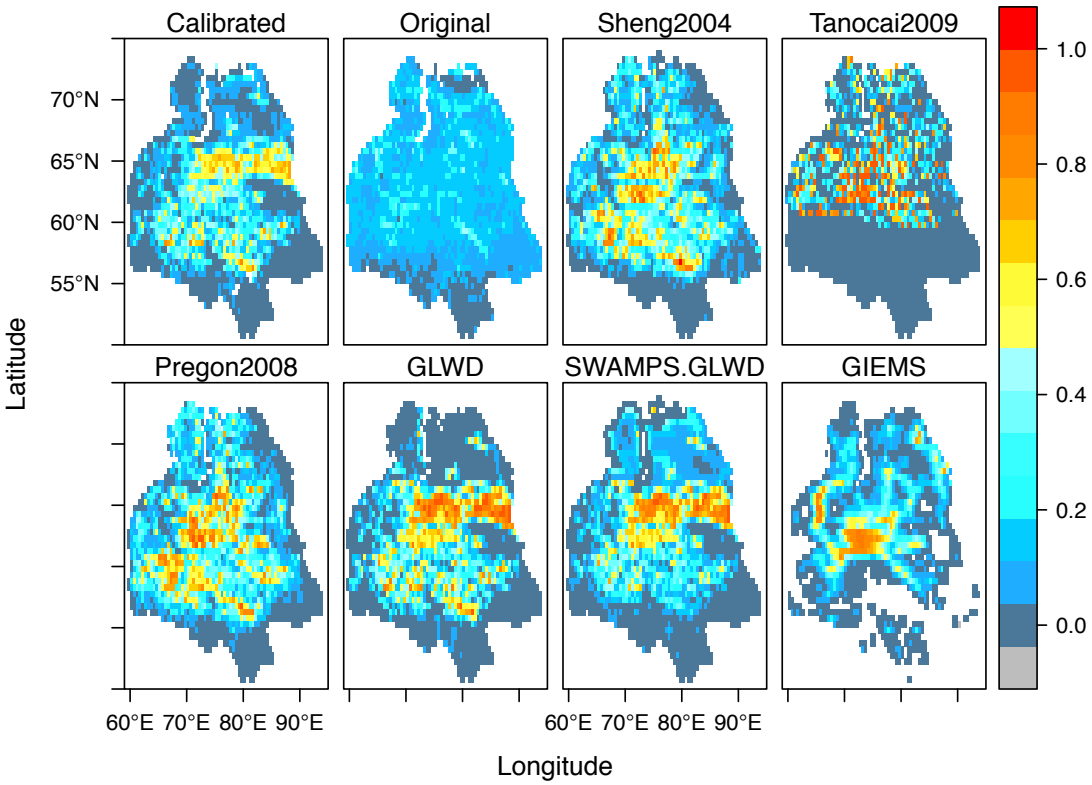

Figure 4 Comparison of TOPMODEL-based wetland areas and Observational datasets over the region West Siberian Lowland (WSL) for June-July-August (JJA) average over the period 1993-2012. 'Calibrated' and 'Original' represent simulated wetland areas with and without F_{max} calibration respectively. For Sheng2004, Tanocai, Pregon2008, and GLWD, it represents maximum wetland extent per 0.5° cell as derived from static inventory maps. For SWAMPS-GLWD and GIEMS, areas shown are averaged for JJA over the period 1993-2007 and 2000-2012 respectively.

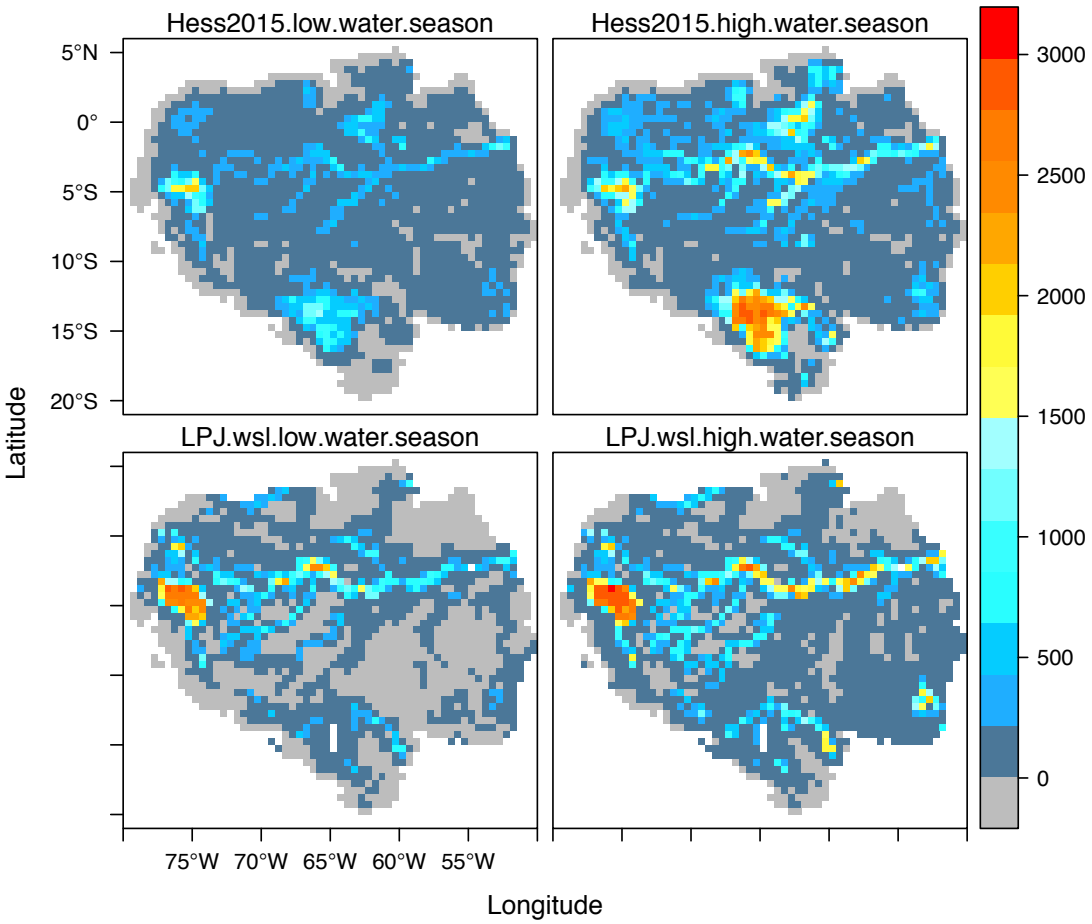

Figure 5. Comparison of wetland areas (km^2) between LPJ-wsl simulated results (SHEDS_basin version) and JERS-1 satellite observation over Lowland Amazon Basin for low-water season and high-water season. The low water season and high-water season in LPJ was calculated by mean annual minimum and maximum respectively during 1993-2013.

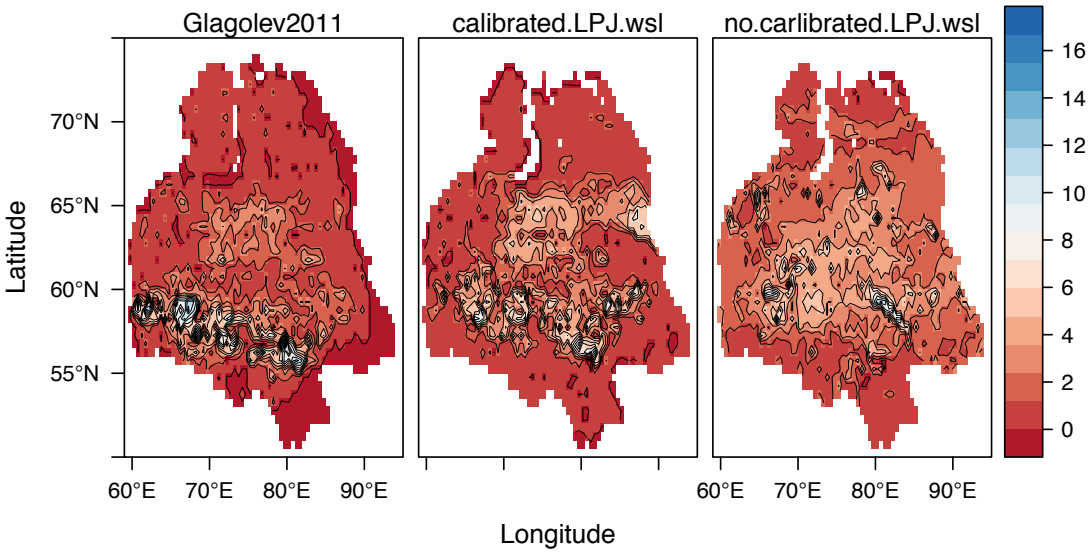

Figure 6. Observation-based estimate from Glagolev et al., 2011 and two LPJ-wsl estimates using Hydro-SHEDS (calibrated F_{max} and non-calibrated F_{max}) for annual CH_4 emission (g CH_4 m^{-2} yr^{-1} of grid cell area). Averages from LPJ-wsl are over the time period 2007-2010.

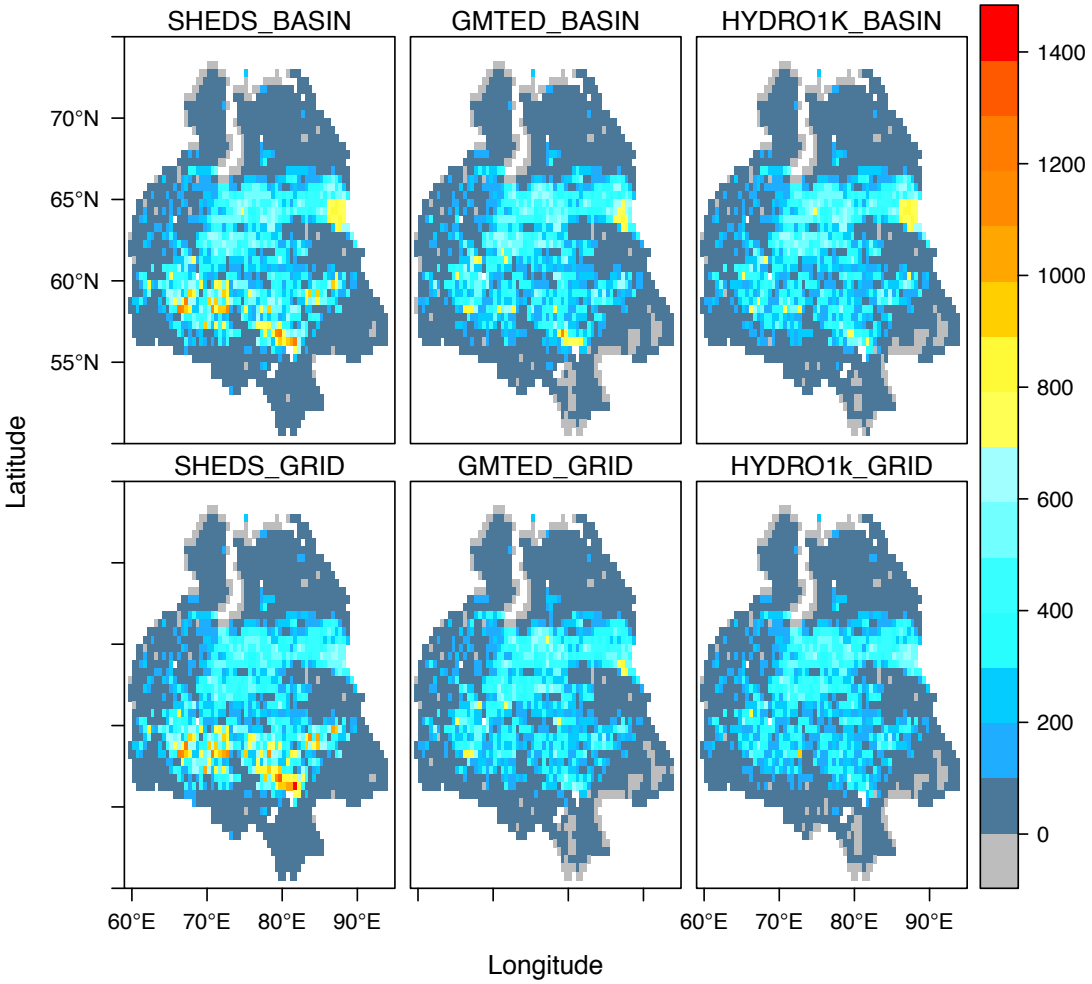

49

50 Figure 7. Spatial distributions of average June-July-August (JJA) wetland area
51 (km^2) over the West Siberian Lowland (WSL) area from model experiments (see
52 Table 2).

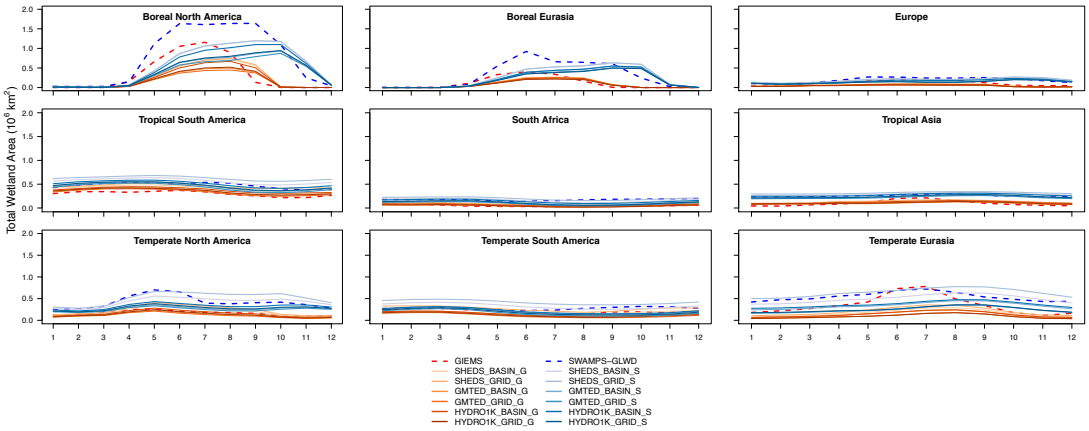

Figure 8. Average seasonal variability of observed and simulated monthly total wetland area for Transcom regions (see Fig. 2). For consistent comparison, two sets of simulated results were generated by masking out pixels for which GIEMS (red, dashed) or SWAMPS-GLWD (blue, dashed) don't have observations (denoted as '-G' and '-S', respectively).

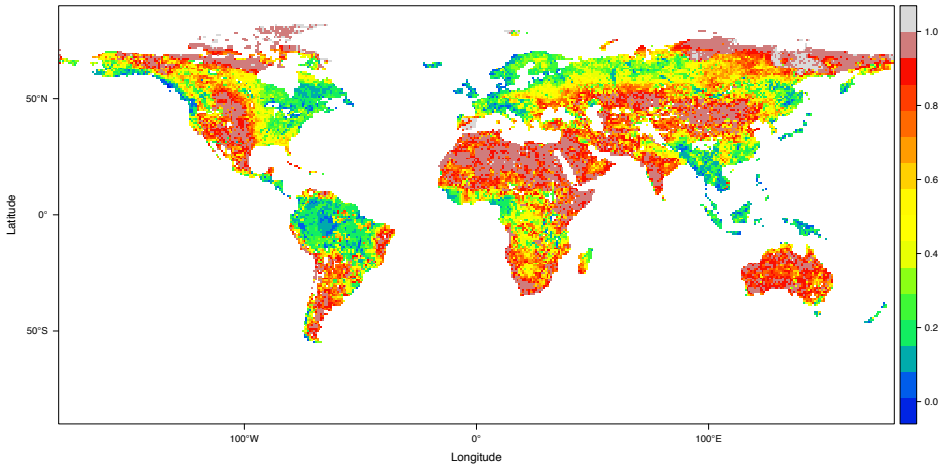

Figure 9. Global wetland potential map, which is calculated by the ratio of the mean annual maximum wetland extent averaged for the time period 1980-2010 and the long-term potential maximum wetland area (F_{max}^{wet}). Higher value represents higher availability for sub-grids to be inundated.

Appendix A

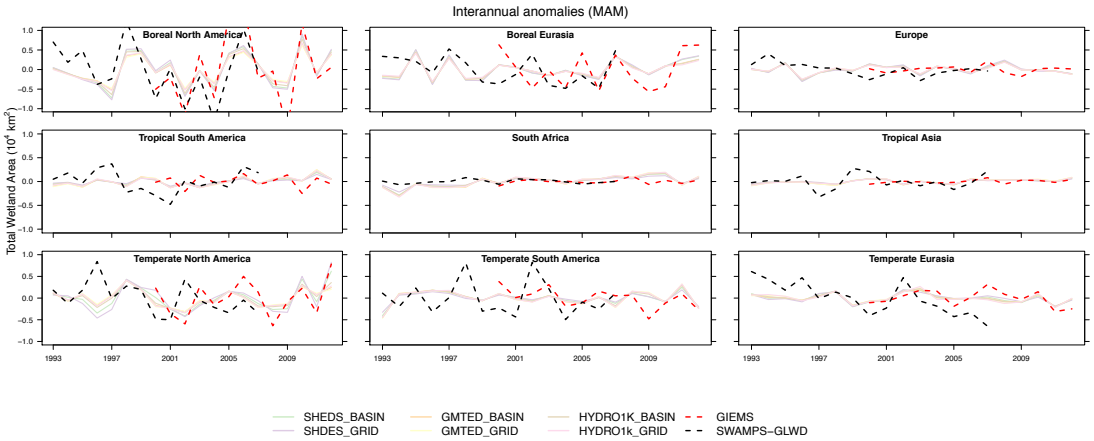
Interannual anomalies (MAM)
Boreal North America
Boreal Eurasia
Europe
Tropical South America
South Africa
Tropical Asia
Temperate North America
Temperate South America
Temperate Eurasia
Total Wetland Area (10^4 km^2)
1993
1997
2001
2005
2009
SHEDS_BASIN
SHDES_GRID
GMTED_BASIN
GMTED_GRID
HYDRO1K_BASIN
HYDRO1k_GRID
GIEMS
SWAMPS−GLWD

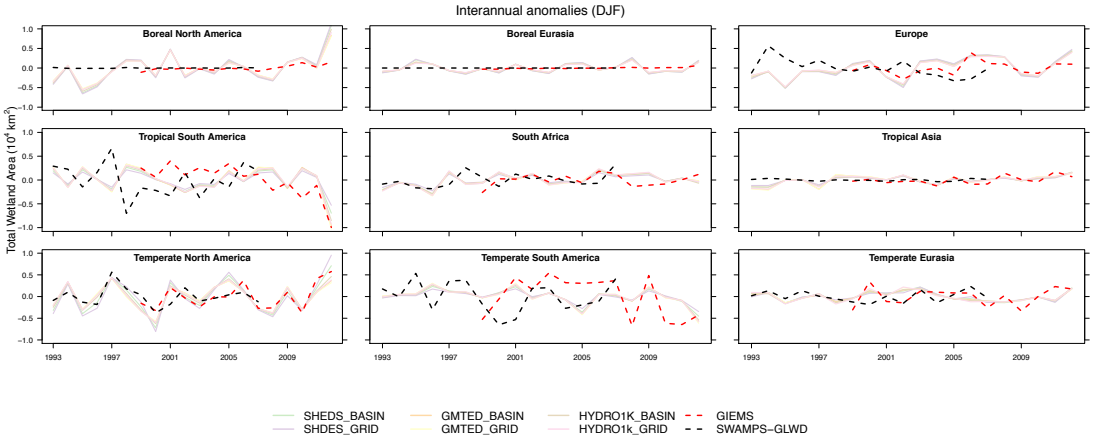
Interannual anomalies (DJF)
Boreal North America
Boreal Eurasia
Europe
Tropical South America
South Africa
Tropical Asia
Temperate North America
Temperate South America
Temperate Eurasia
Total Wetland Area (10^4 km^2)
1993
1997
2001
2005
2009
SHEDS_BASIN
SHDES_GRID
GMTED_BASIN
GMTED_GRID
HYDRO1K_BASIN
HYDRO1k_GRID
GIEMS
SWAMPS−GLWD

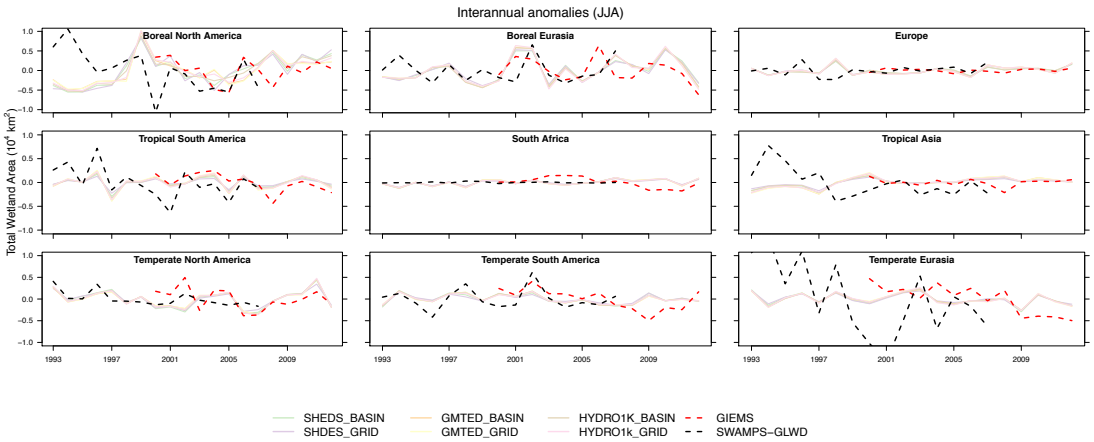
Interannual anomalies (JJA)
Boreal North America
Boreal Eurasia
Europe
Tropical South America
South Africa
Tropical Asia
Temperate North America
Temperate South America
Temperate Eurasia
Total Wetland Area (10^4 km^2)
1993
1997
2001
2005
2009
SHEDS_BASIN
SHDES_GRID
GMTED_BASIN
GMTED_GRID
HYDRO1K_BASIN
HYDRO1k_GRID
GIEMS
SWAMPS−GLWD

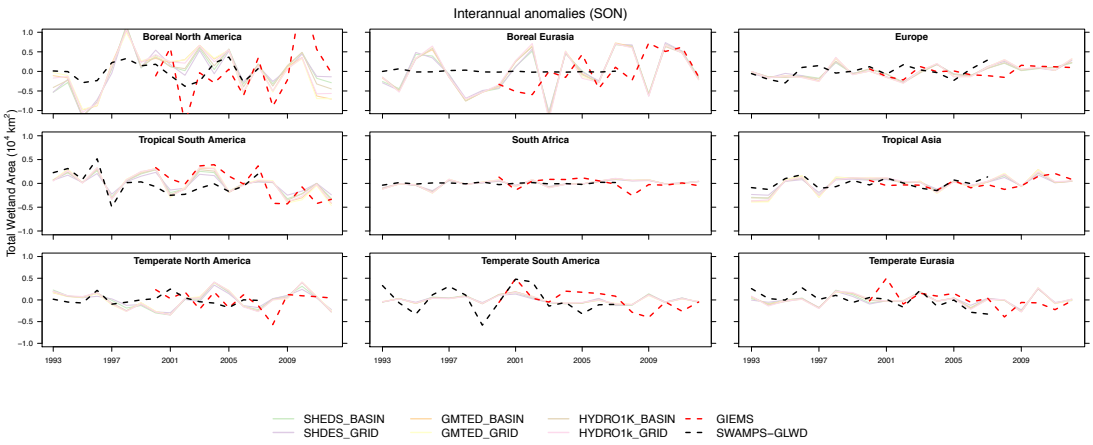

Figure A1. Interannual variations of seasonal wetland area anomalies from LPJ-wsl and satellite-derived observations for the period 1993-2012.

Table A1. Reclassification table for aggregating JERS-1 lowland Amazon basin to 0.5° cell. Code NA, 0, 1, and 2 represent Not-Available, Not Wetlands, wetland only exist in low-water season and wetland exist in high-water season.

DN	Cover at low-water stage	Cover at higher-water stage	Flag for minimum/ maximum wetlands
0	Land outside Amazon Basin	Land outside Amazon Basin	NA
1	Non-wetland within Amazon Basin	Non-wetland within Amazon Basin	0
11	Open water	Open water	0
13	Open water	Aquatic macrophyte	0
21	Bare soil or herbaceous, non-flooded	Open water	2
23	Bare soil or herbaceous, non-flooded	Aquatic macrophyte	2
33	Aquatic macrophyte	Aquatic macrophyte	1
41	Shrub, non-flooded	Open water	2
44	Shrub, non-flooded	Shrub, non-flooded	0
45	Shrub, non-flooded	Shrub, flooded	2
51	Shrub, flooded	Open water	1
55	Shrub, flooded	Shrub, flooded	1
66	Woodland, non-flooded	Woodland, non-flooded	0
67	Woodland, non-flooded	Woodland, flooded	2

77	Woodland, flooded	Woodland, flooded	1
88	Forest, non-flooded	Forest, non-flooded	0
89	Forest, non-flooded	Forest, flooded	2
99	Forest, flooded	Forest, flooded	1
200	Elevation >= 500m, in Basin	Elevation >= 500, in Basin	NA
255	Ocean	Ocean	NA